Earthquake Geotechnical Engineering

Part II: SOILS DYNAMIC RESPONSE

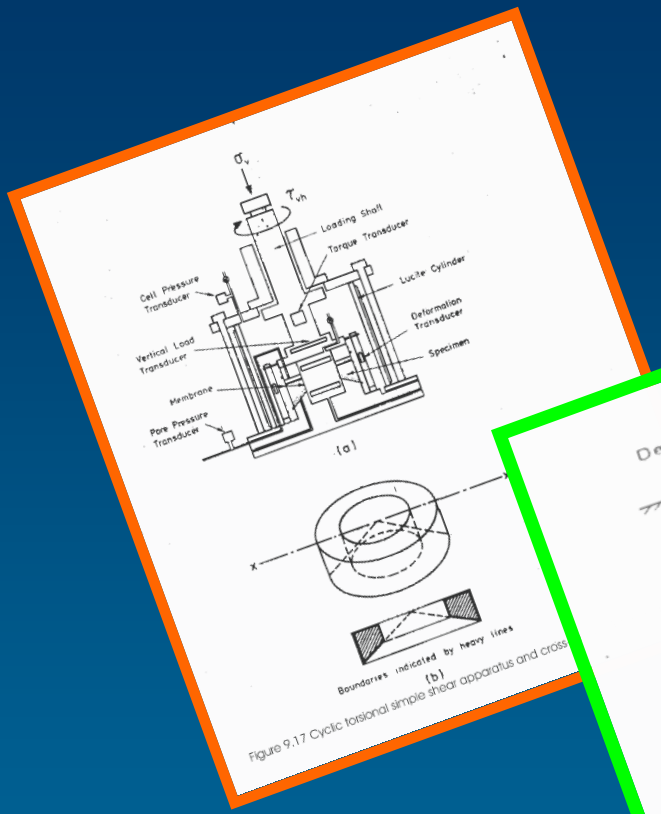

Figure 9.17 Cyclic torsional simple shear apparatus and cross

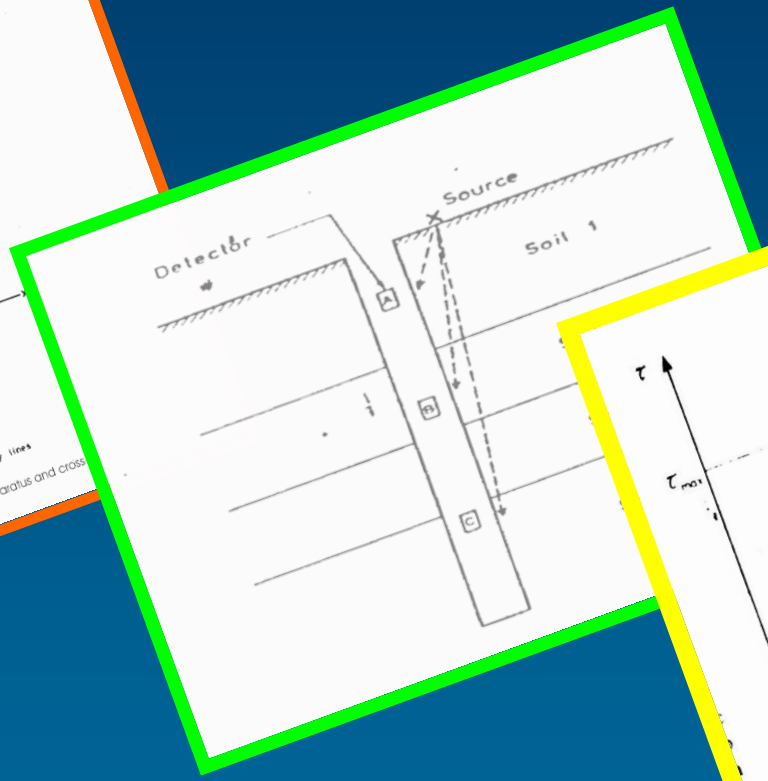

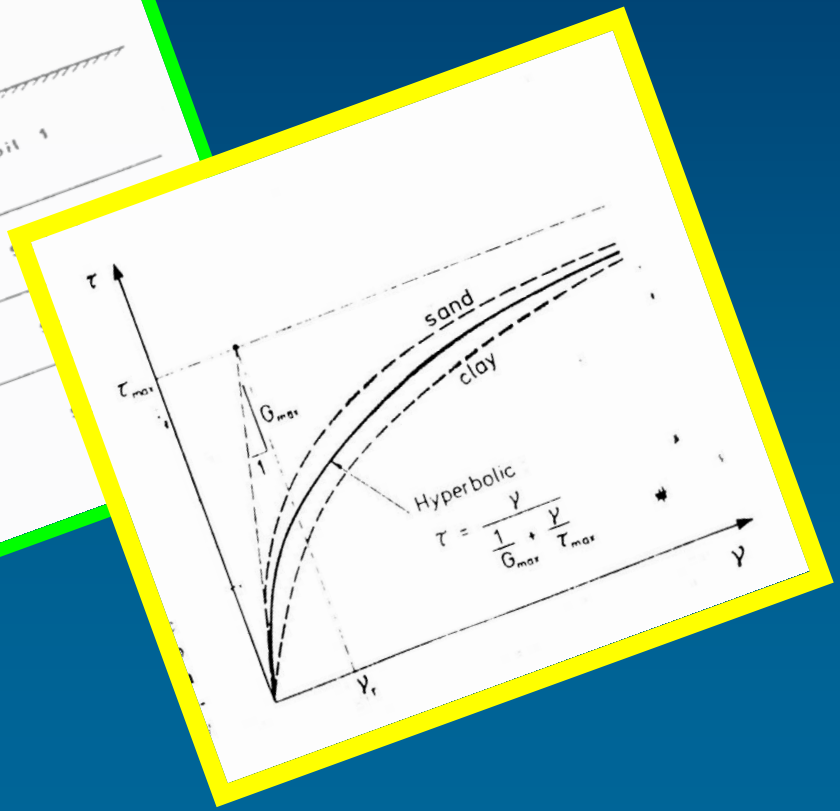

Facultad de Ingeniería de la Universidad Nacional de Cuyo

Dynamic Soils Properties

Soils' static response depends on the following factors at least:

- ❑ Type of soil (gravels, sands, silts, clays) and its properties: grain size distribution, plasticity, shear resistance parameters, permeability, etc.
- ❑ Unit weight ("density").
- ❑ Water content.
- ❑ Stress path.
- ❑ Stress history.

Those factors influence the dynamic response in a greater extent. There are other influent topics.

Dynamic Stiffness

In mechanical soil response, both shear strains and stresses are the most relevant parameters to be taken into account.

Basic stress – strain relationships in linear elastic materials are the followings:

$$\tau[MPa] = G[MPa] * \gamma[\%]$$

The shear modulus **G** at least depends on:

- Relative density Dr
- Shear strain γ
- Strain history
- Effective confinement stress σ'_{v0}

Emerges the following idea:

- ➔At origin tangent G: $G_{máx}$ or G_0
- ➔Secant G
- ➔Local tangent G

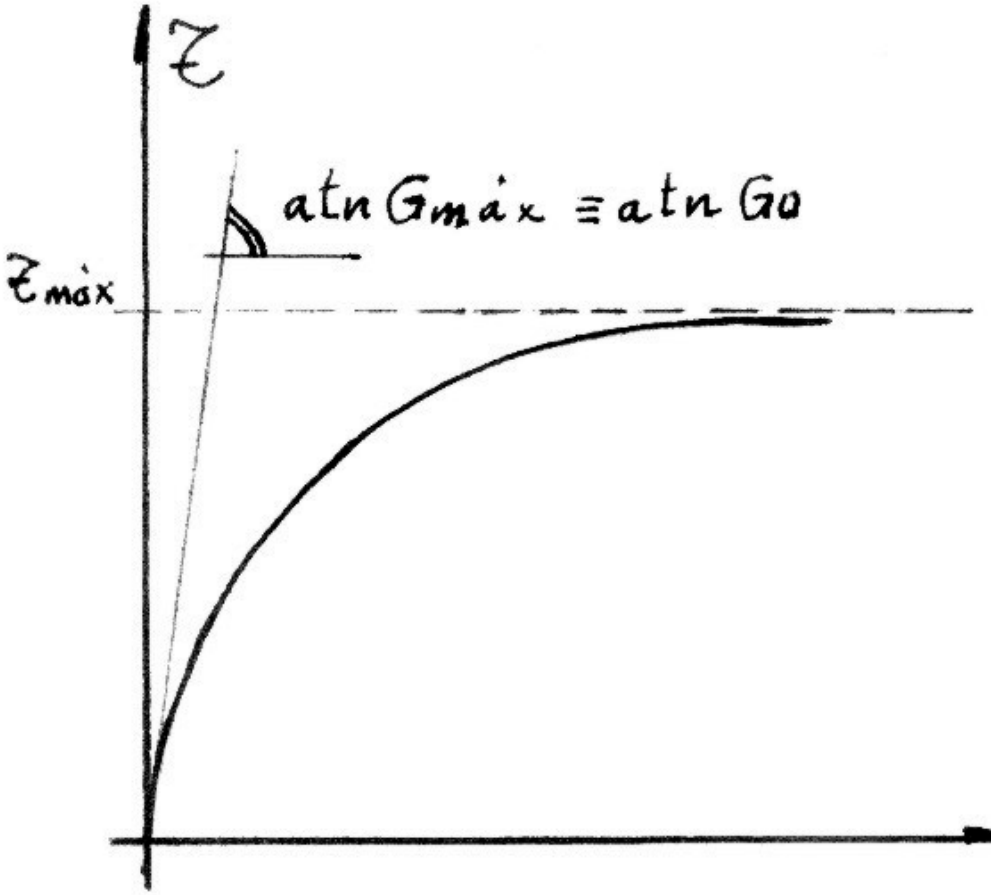

Hardin & Drnevich have proposed the following simplified expressions:

- Sands: $G_{max} = K_2 * (\sigma'_0)^{1/2}$

- Clays: $G_{máx} = \frac{3230 * (2{,}973 - e)^2}{(1 + e)} * OCR^k * (\sigma'_0)^{½}$

Plasticity index [%]	K
0	0,00
20	0,18
40	0,30
60	0,41
80	0,48
>100	0,50

Despite each soil has particular characteristics, generally occurs that:

- **In sands, G depends strongly on Dr.**
- **In clays, G depends strongly on OCR.**
- **G depends strongly on γ specially if**

$$\gamma > 1E\text{-}04 \quad \text{or} \quad \gamma > 1E\text{-}05$$

- **The frequency of vibration has only an irrelevant influence.**

Damping:

Cyclic loading and unloading generates a loop whose area means the wasted energy in the process.

There are different types of damping:

- ❑ Radiation or geometric damping.
- ❑ Viscous material damping (proportional to the strain velocity).
- ❑ Hysteretic material damping (grows with the number of cycles).

In soils geometric and hysteretic damping are dominant.

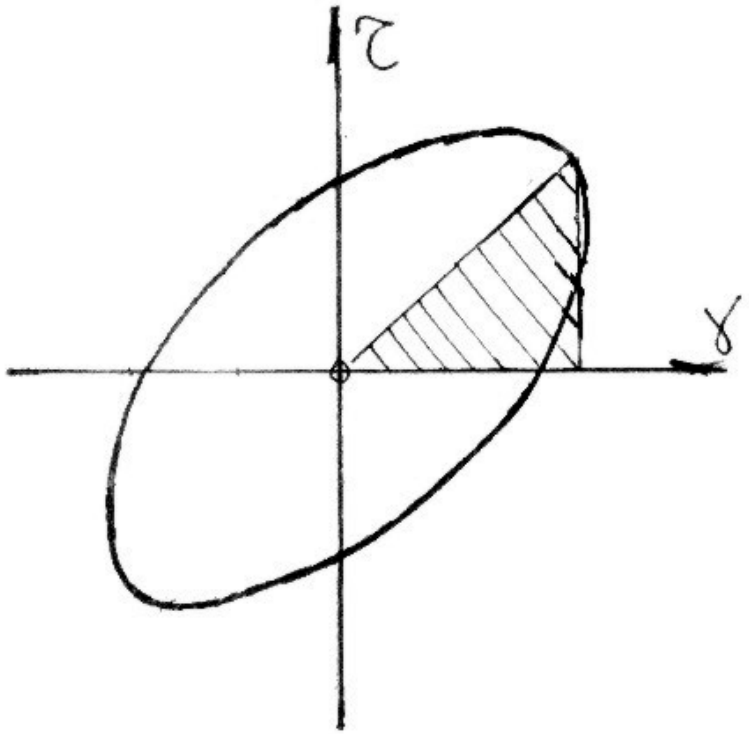

Relative damping can be defined as follows:

$$x = \frac{\text{Max energy dissipated (loop)}}{4\pi * \text{Max strain energy (triangle)}} = \frac{A_{loop}}{2\pi\, G_{sec} * \gamma_c^2}$$

Expression that doesn't depends on the frequency.

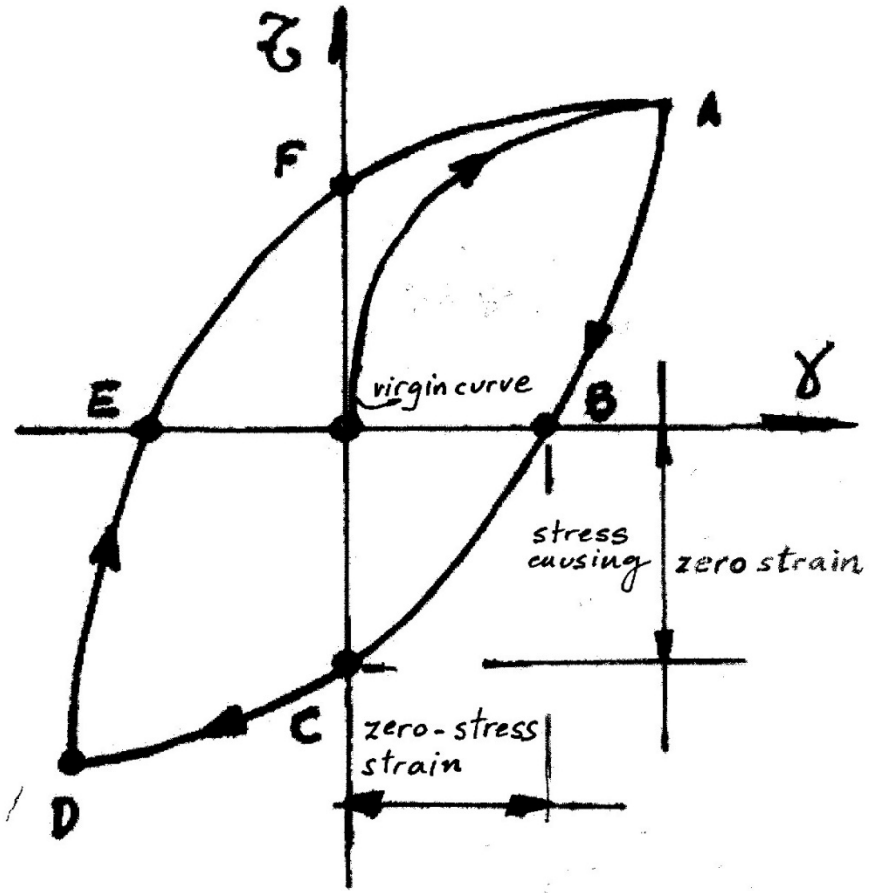

Mathematical Models for Soil Dynamic Response

It is necessary to count on stress – strain relationships to model the soil development. Classical expressions are the following:

Classical expressions mathematical models are:

- **Kodner - Zelasko (1963):**

$$\frac{1}{G} = \frac{1}{G_0} * \left(1 + G_0 * \frac{G_0 * \gamma}{\tau_{max}}\right)$$

- **Ramberg – Osgood (1943)**

$$\frac{\gamma}{\gamma_y} = \frac{\tau}{\tau_\psi} * \left[1 + \alpha * \left(\frac{\gamma}{C * \tau_y}\right)^{-R}\right]$$

Usual values

Soil	R	a	C
Sand	3 ÷ 5	1 ÷ 2	0,8
Clay	3	1	0,4

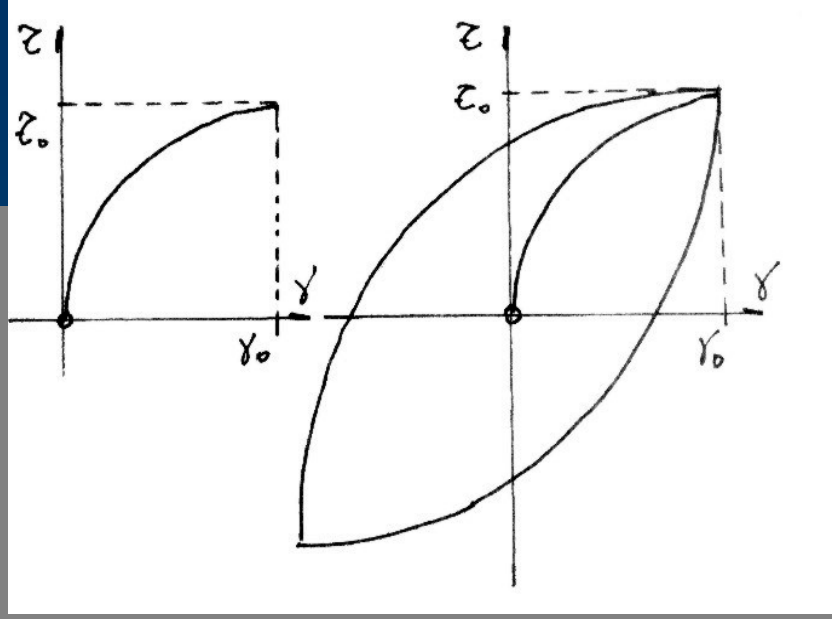

- "Type Massing" response (1926),
- whose principal characteristics are:
  - ✓The discharge - recharge curves are similar to the "virgin curve".
  - ✓The maximum shear modulus

G_0 ≈ initial shear modulus of each stress – strain cycle.

$$\text{If } \tau = F(\gamma) \quad \Rightarrow \quad \frac{\tau_0 - \tau}{2} = F\left(\frac{\gamma_0 - \gamma}{2}\right)$$

where (τ_0,γ_0) and (τ_0,γ_0) are the extremes of the discharge recharge loop.

That is equivalent to put the origin at the extreme of the loop [point (τ_0,γ_0)], and draw the discharge line at double scale.

The method allows having a loop for each point (τ_0,γ_0).

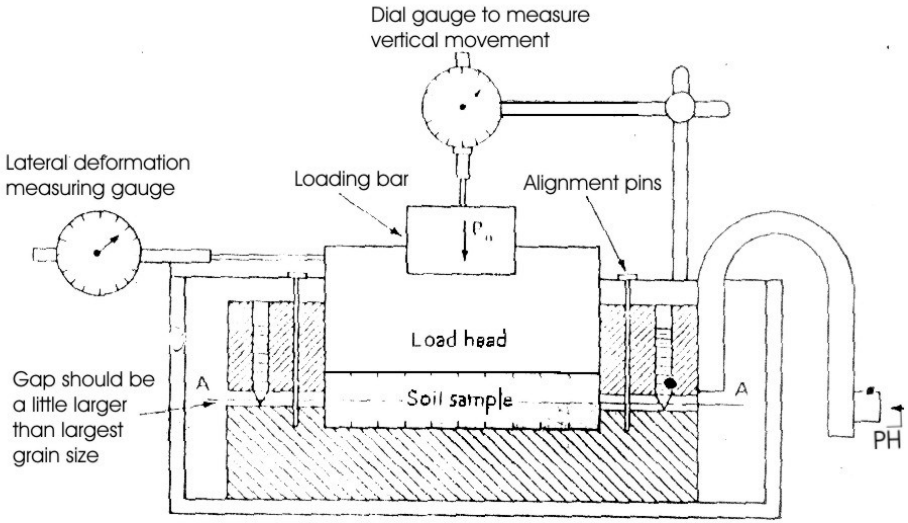

Figure 4.1 Direct shear apparatus.

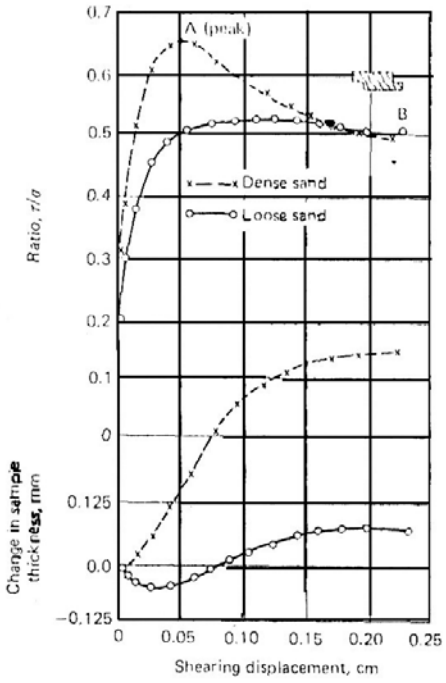

(a)

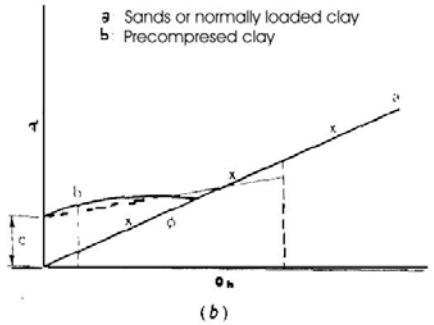

(b)

Figure 4.2 (a) Typical direct shear data for sands. (From D. W. Taylor: Fundamentals of Soil Mechanics by permission of Jhon Wiley and Sons, Inc., New York.) (b) Mohr strength envelopes from direct shear test.

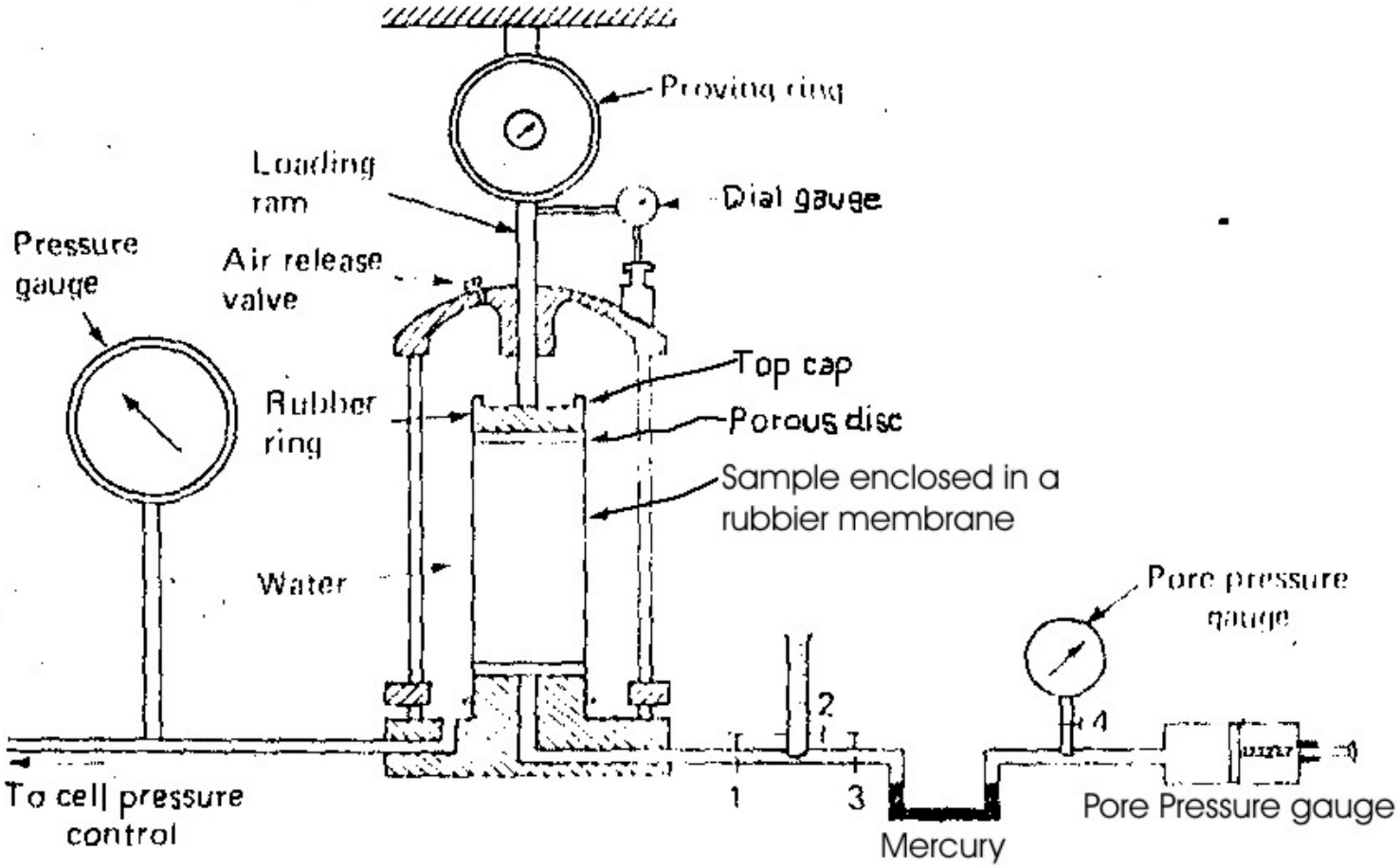

Figure 4.3 Triaxial apparatus.

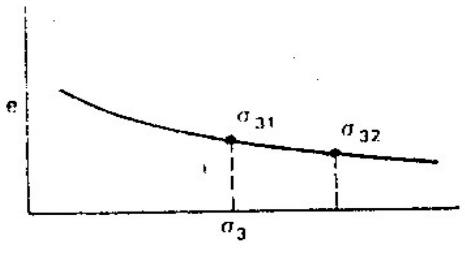

(a)

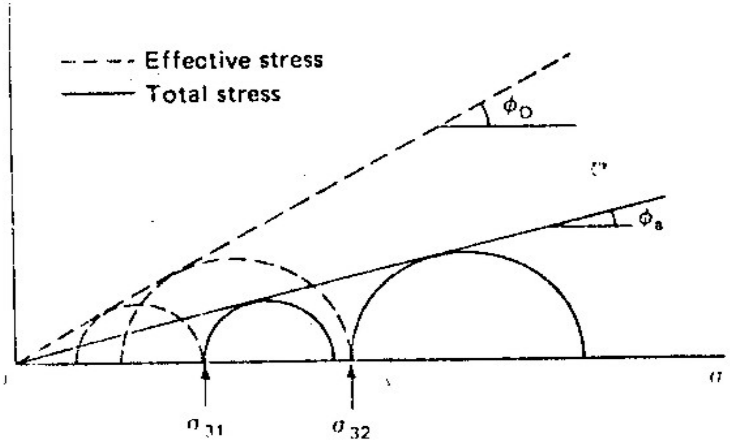

(b)

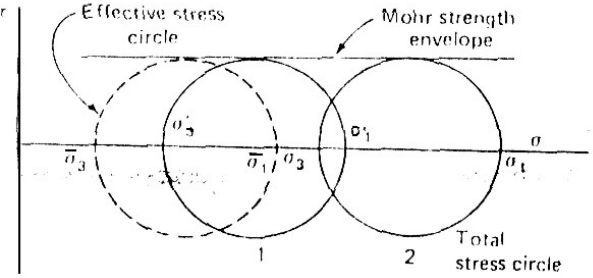

Figure 4.4 Mohr plot for undrained test.

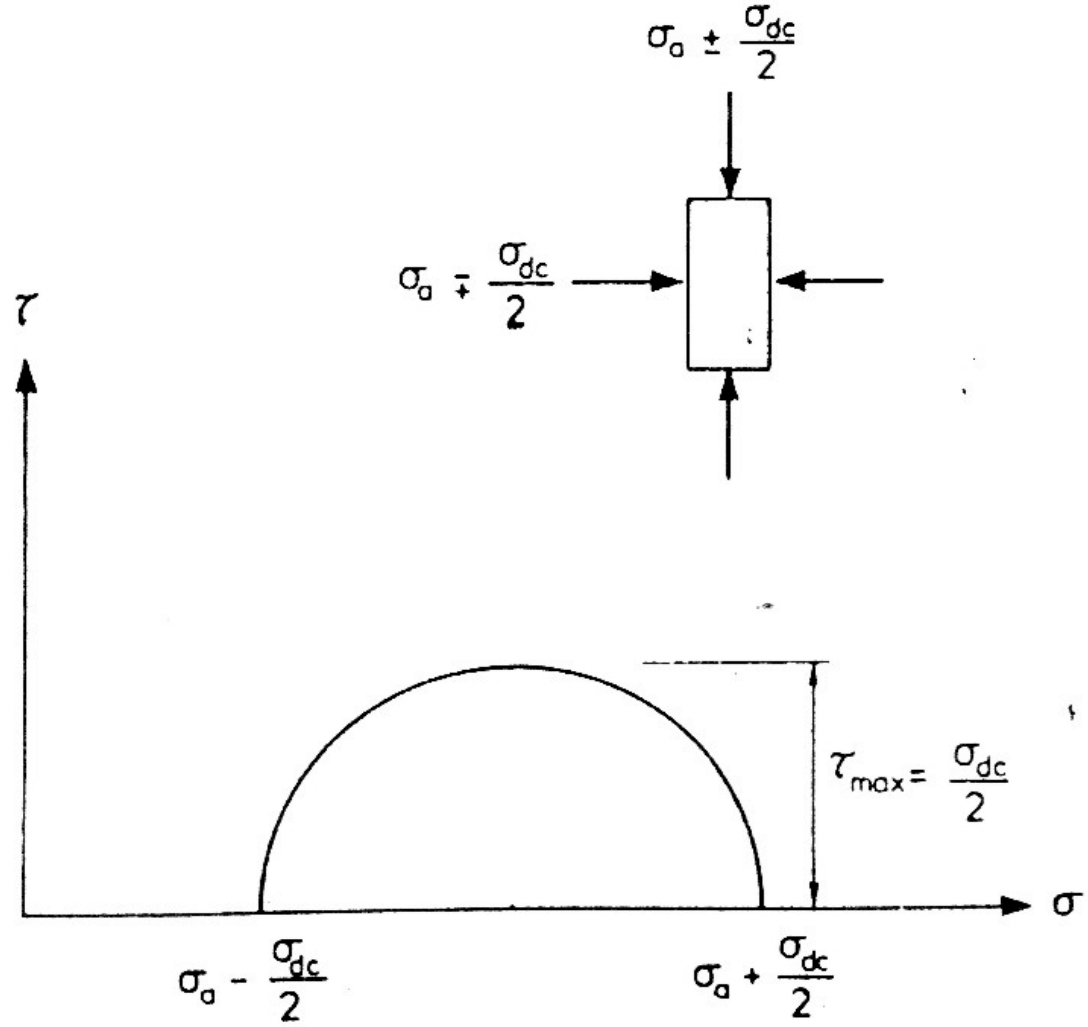

Figure 9.12. Cyclic triaxial compression stress conditions.

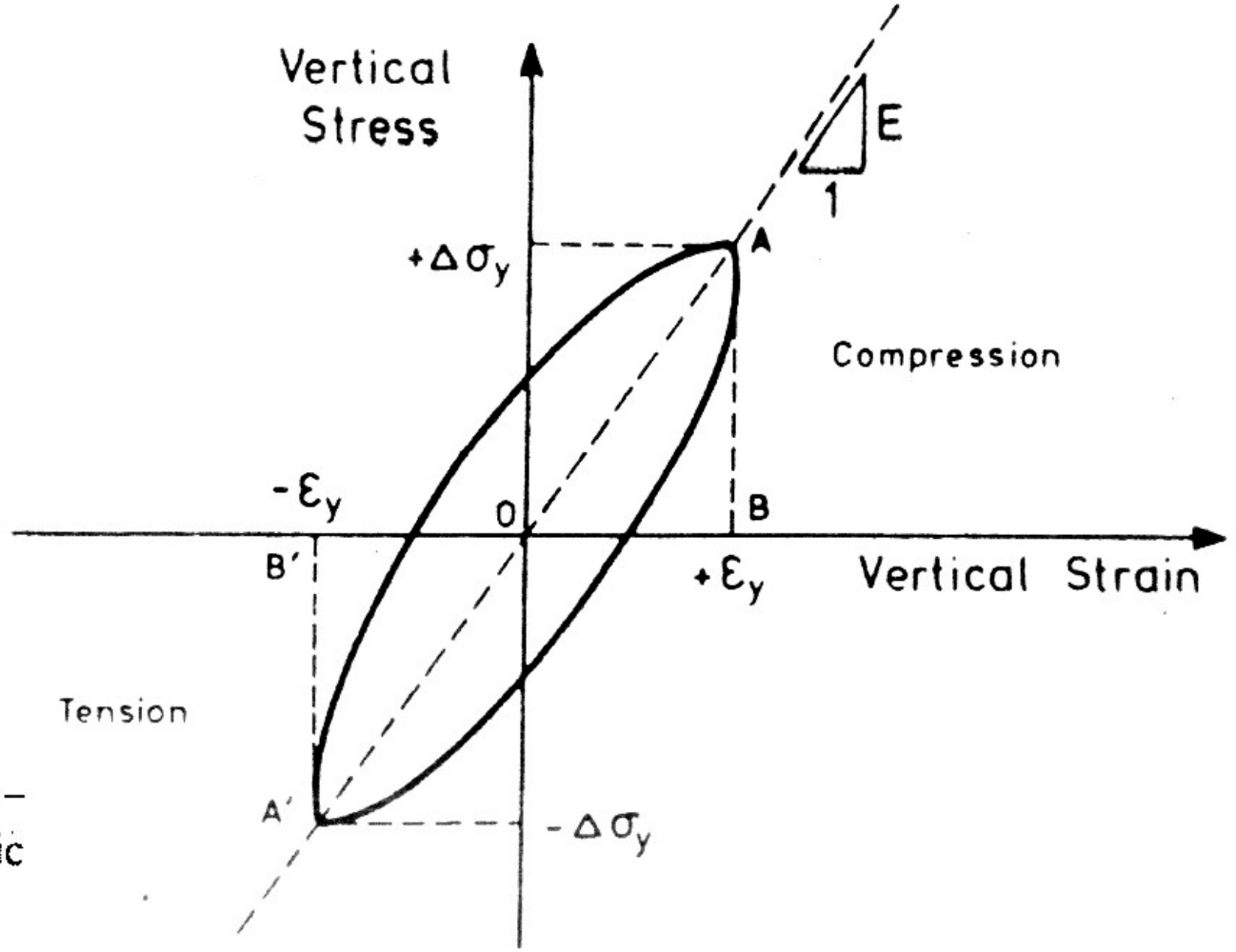

Figure 9.13. Typical stress–strain behaviour in a cyclic triaxial test.

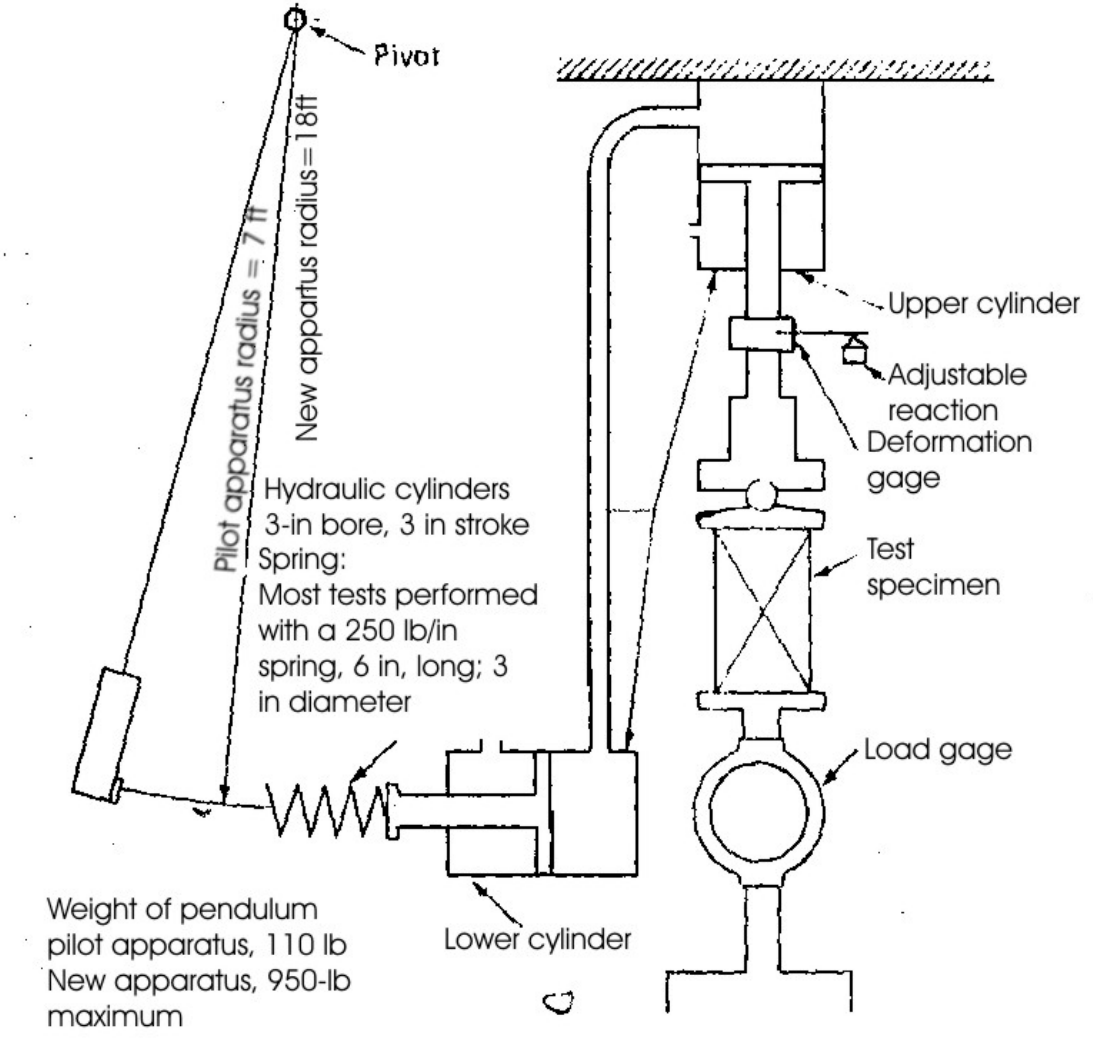

Figure 4.6 Pendulum loading apparatus. (After Casagrande and Shannon, 1948b.)

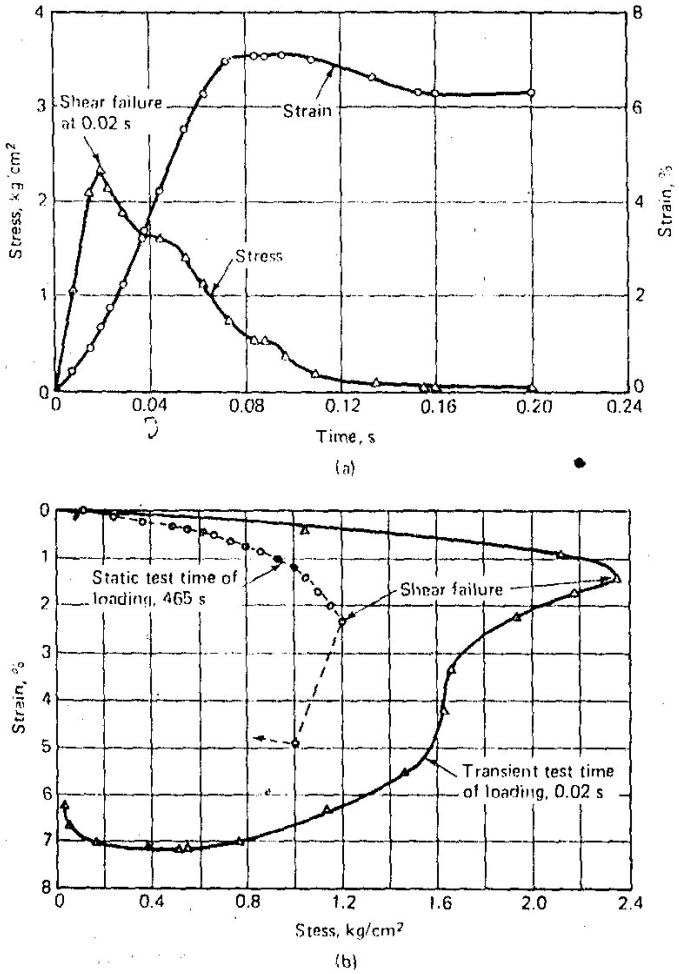

Figure 4.8 (*a*) Time vs. stress and strain in an unconfined transient test on Cambridge clay. (*b*) Stress vs. strain in transient test with time of loading of 0.02 s and a static test on Cambridge clay. *(After Casagrande and Shannon, 1949.)*

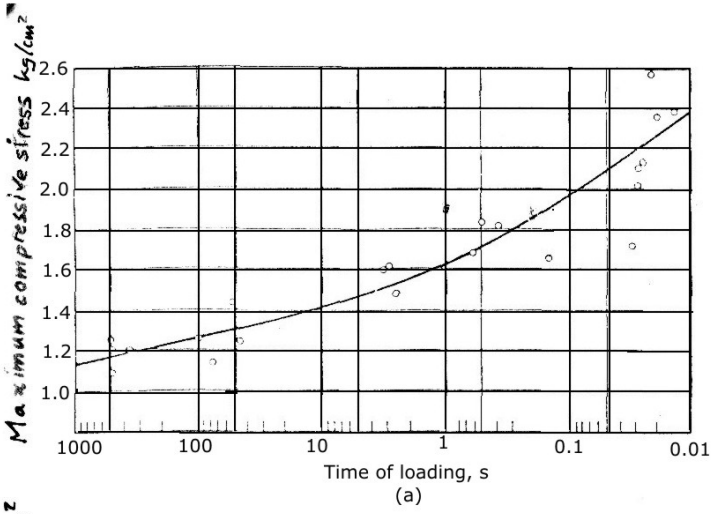

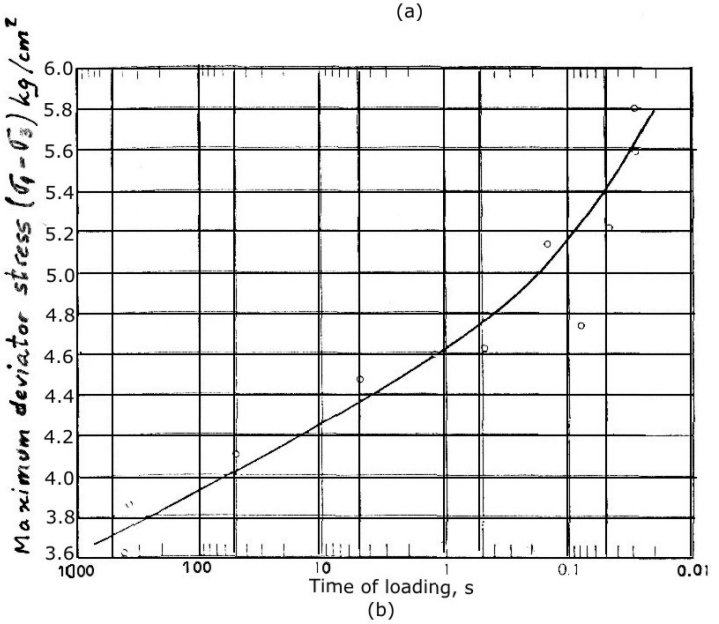

Figure 4.9 (a) Maximum compressive stress vs. time of loading in unconfined compression test on Cambridge clay. (b) Maximum compresive stress vs. time of loading in confined compression test on Cambridge clay. (After Casagrande and Shannon, 1949.)

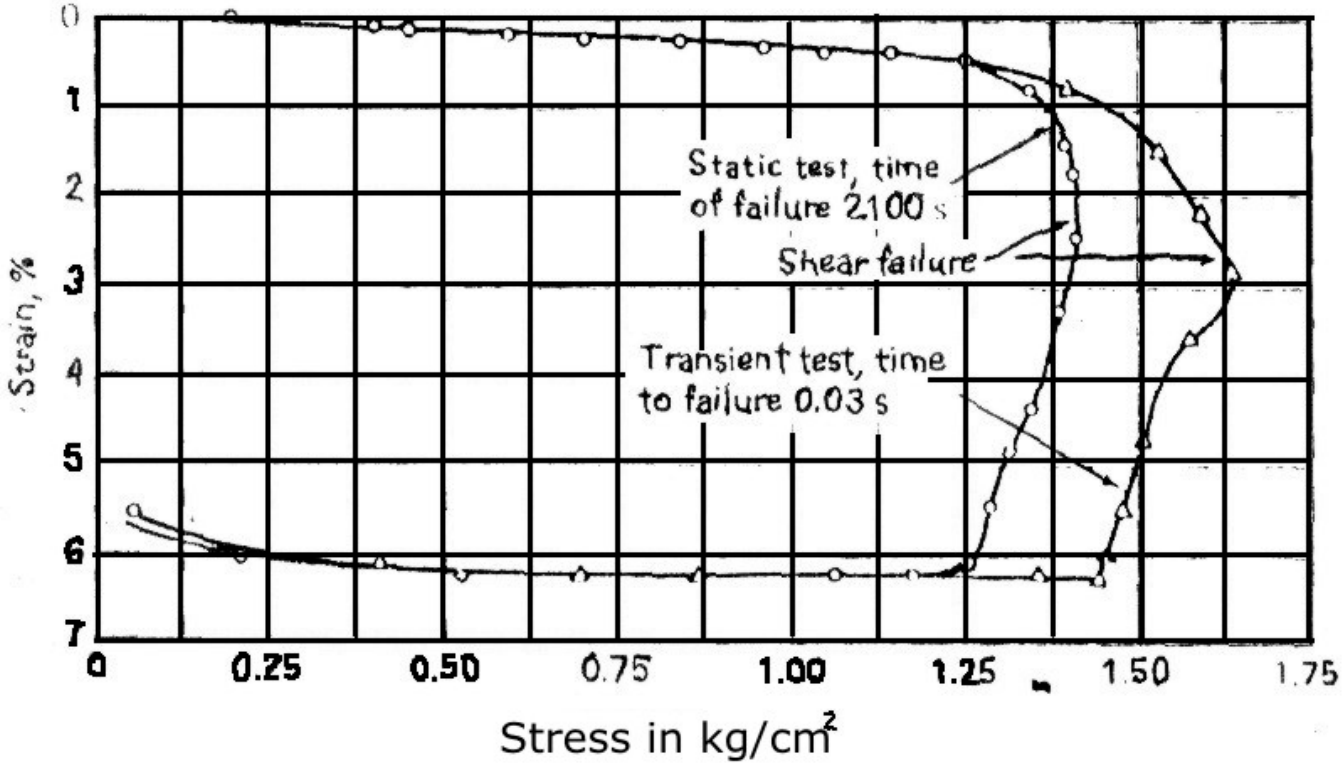

Figura 5.10 Stress vs. strain of Manchester sand in a transient test and static. (After Casagrande and Shannon 1949.)

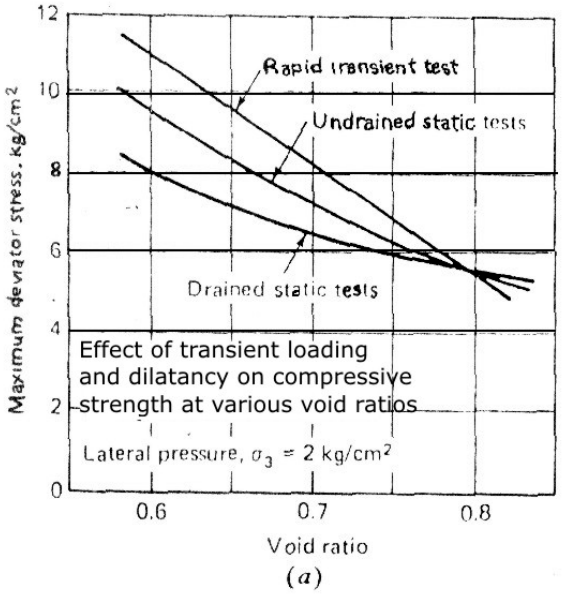

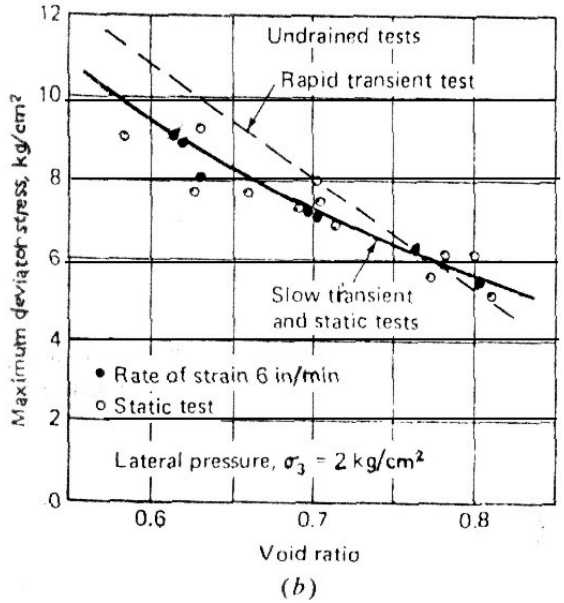

Figure 4.12 Maximum deviator stress vs. void ratio of Sacramento sand. (a) Drained static, undrained static, and rapid transient both drained and undrained. (b) Undrained rapid transient and slow transient and static test. (After Seed and Lundgren, 1954. Reprinted with permission of ASTM, Philadelphia, Pa.)

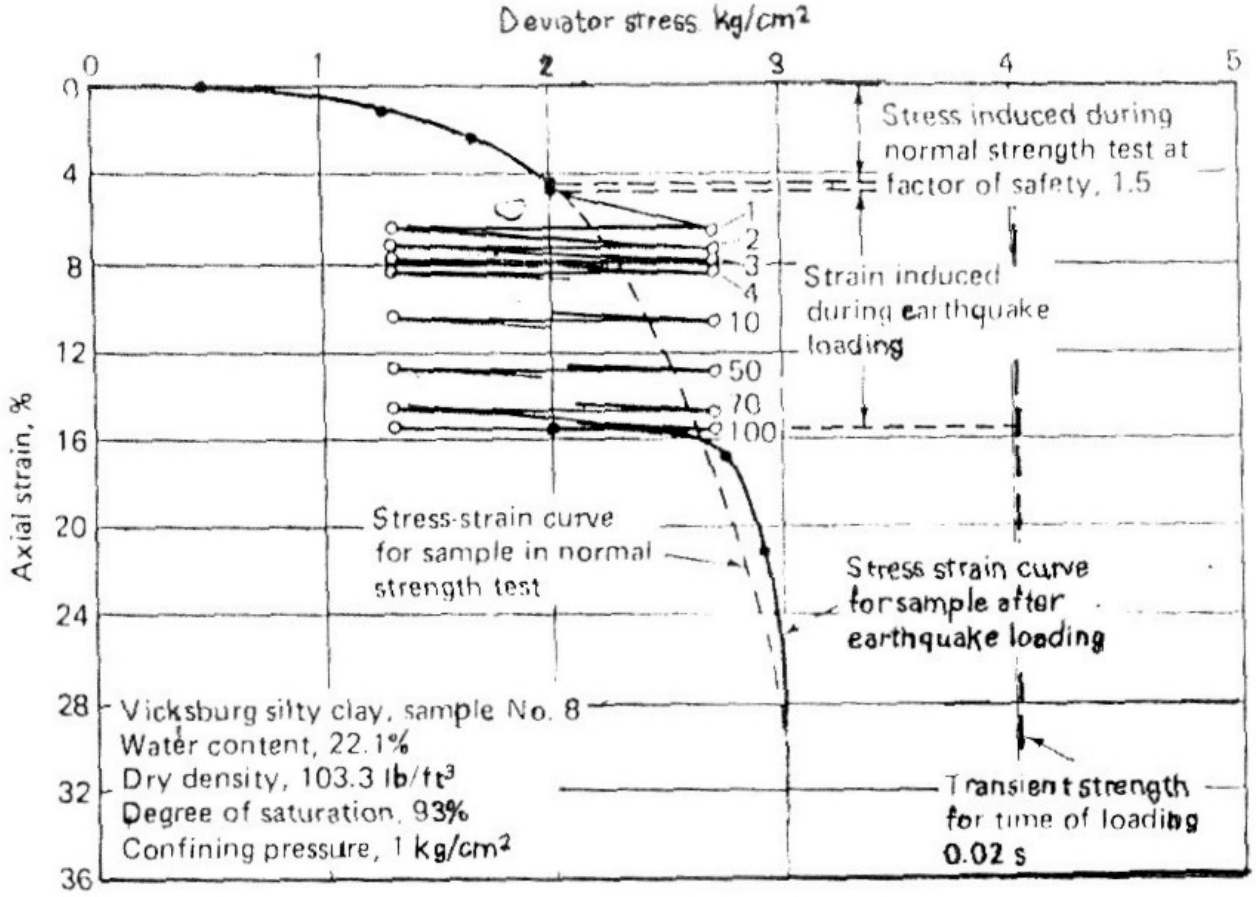

Figure 4.14 Stress vs. strain for Vicksburg silty clay under applied static and oscillatory stress in triaxial test. *(After Seed, 1960.)*

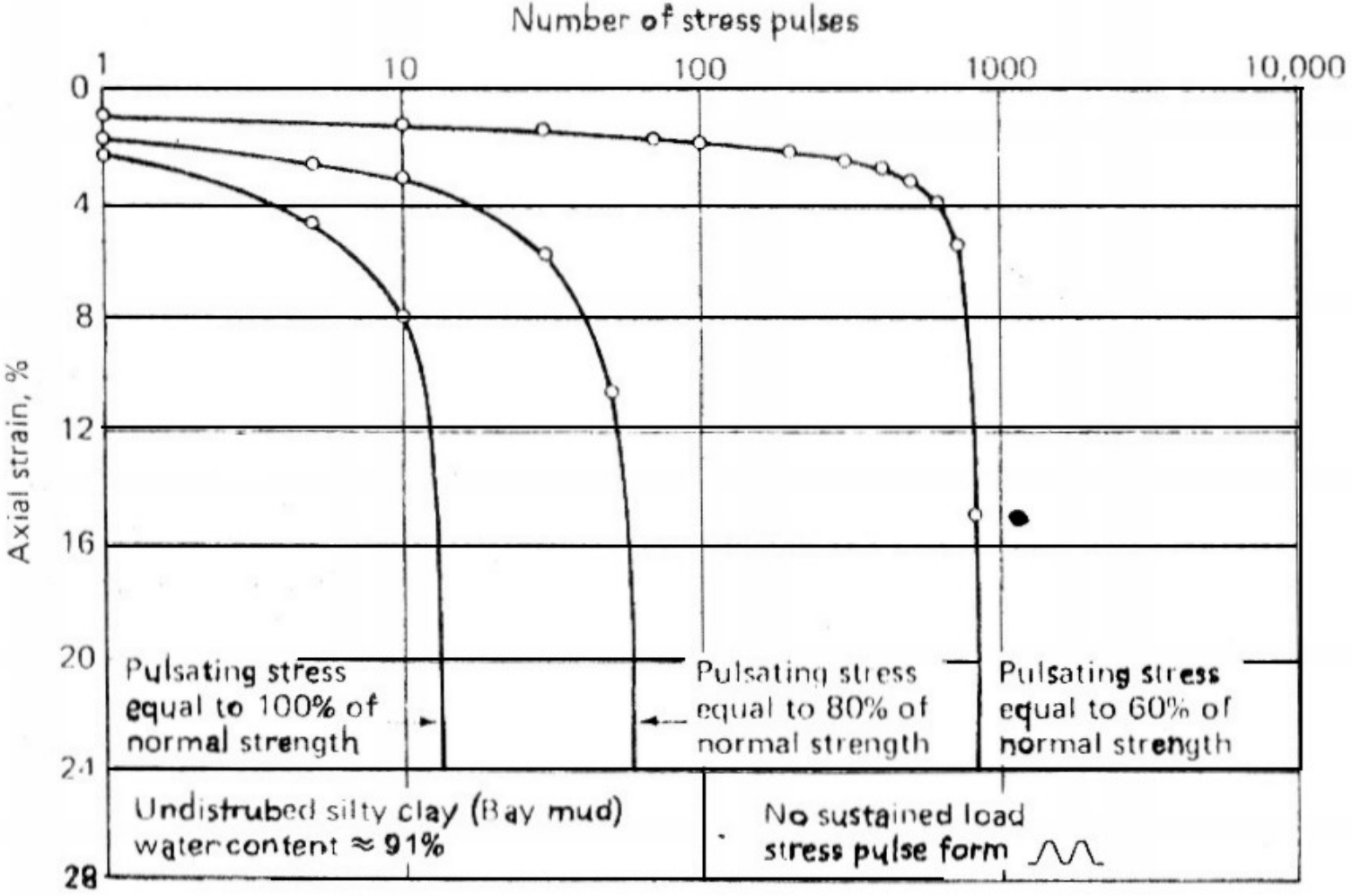

Figure 4.15 Soil deformation under pulsating stress applications in one-directional loading. *(After Seed and Chan, 1966.)*

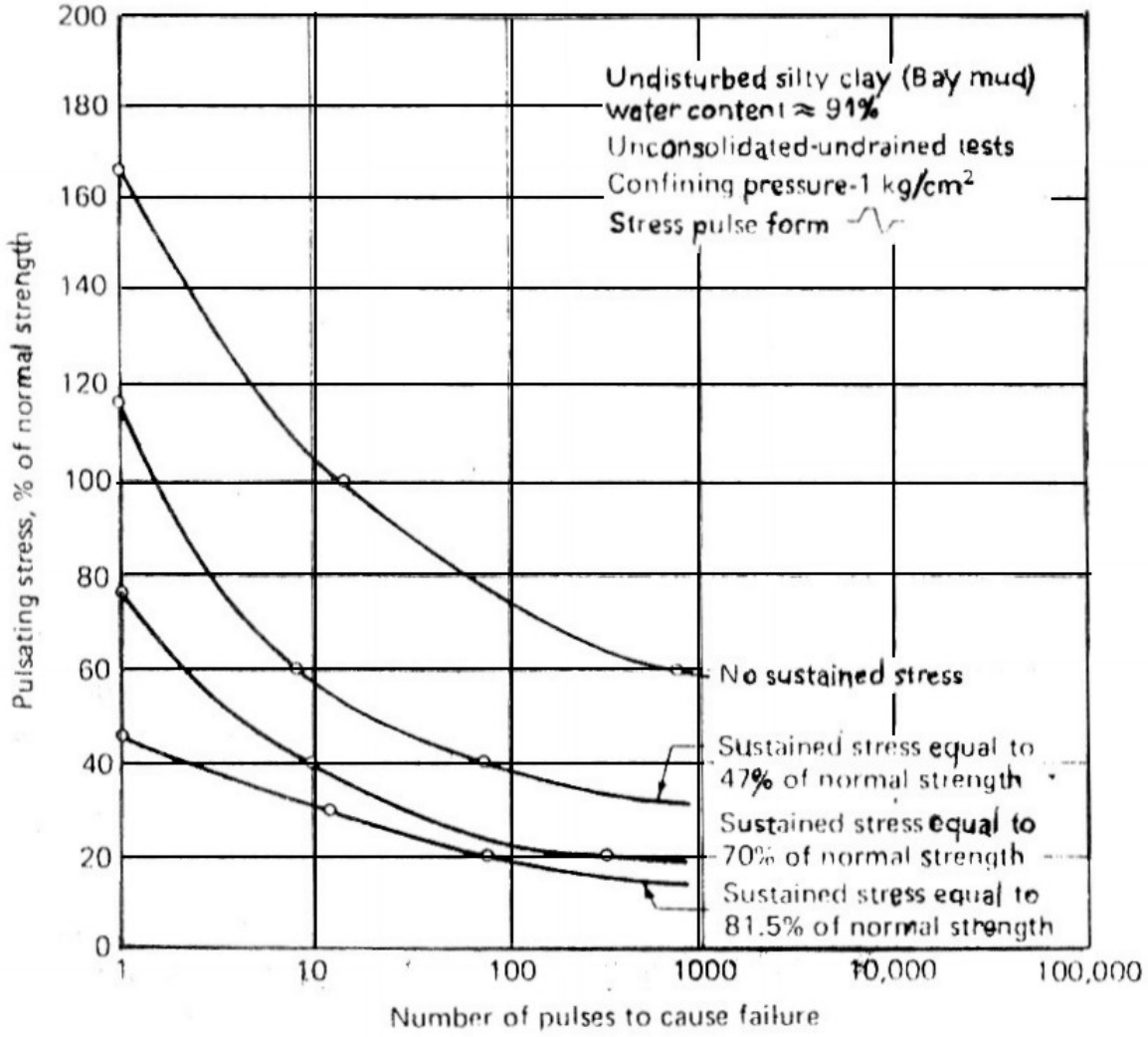

Figure 4.16 Relationship between stress level and number of pulses causing failure in one-directional loading. *(After Seed and Chan, 1966.)*

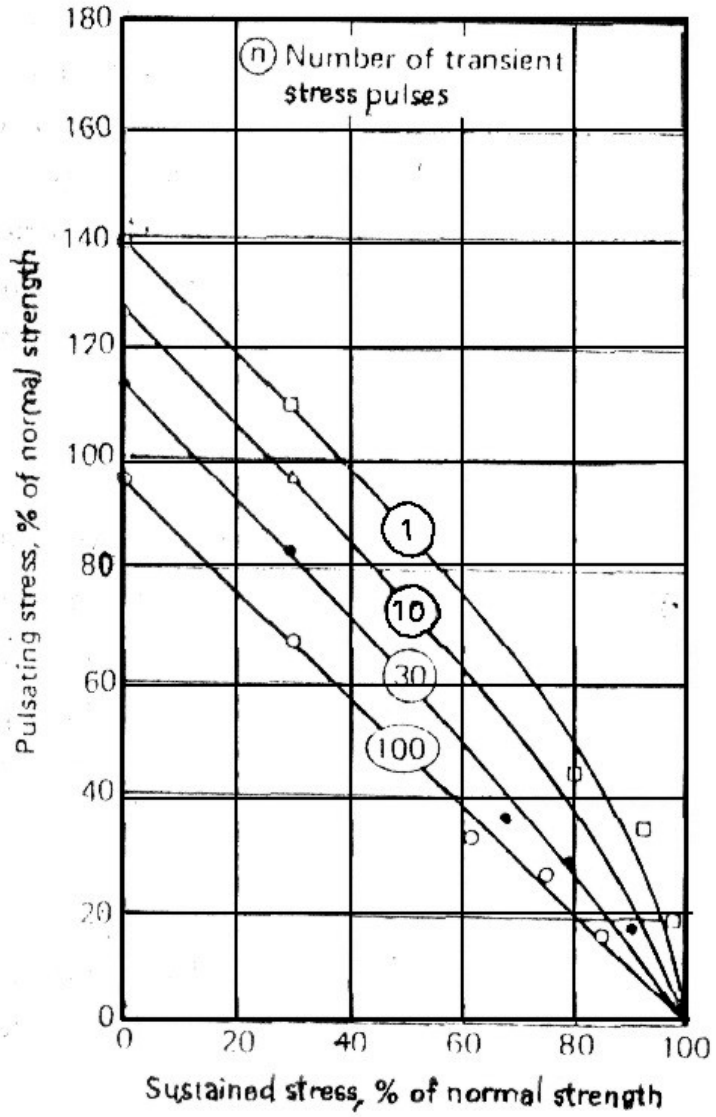

Figure 4.17 Combination of sustained and pulsating stress intensities causing failure in Vicksburg silty clay. (*After Seed and Chan, 1966.*)

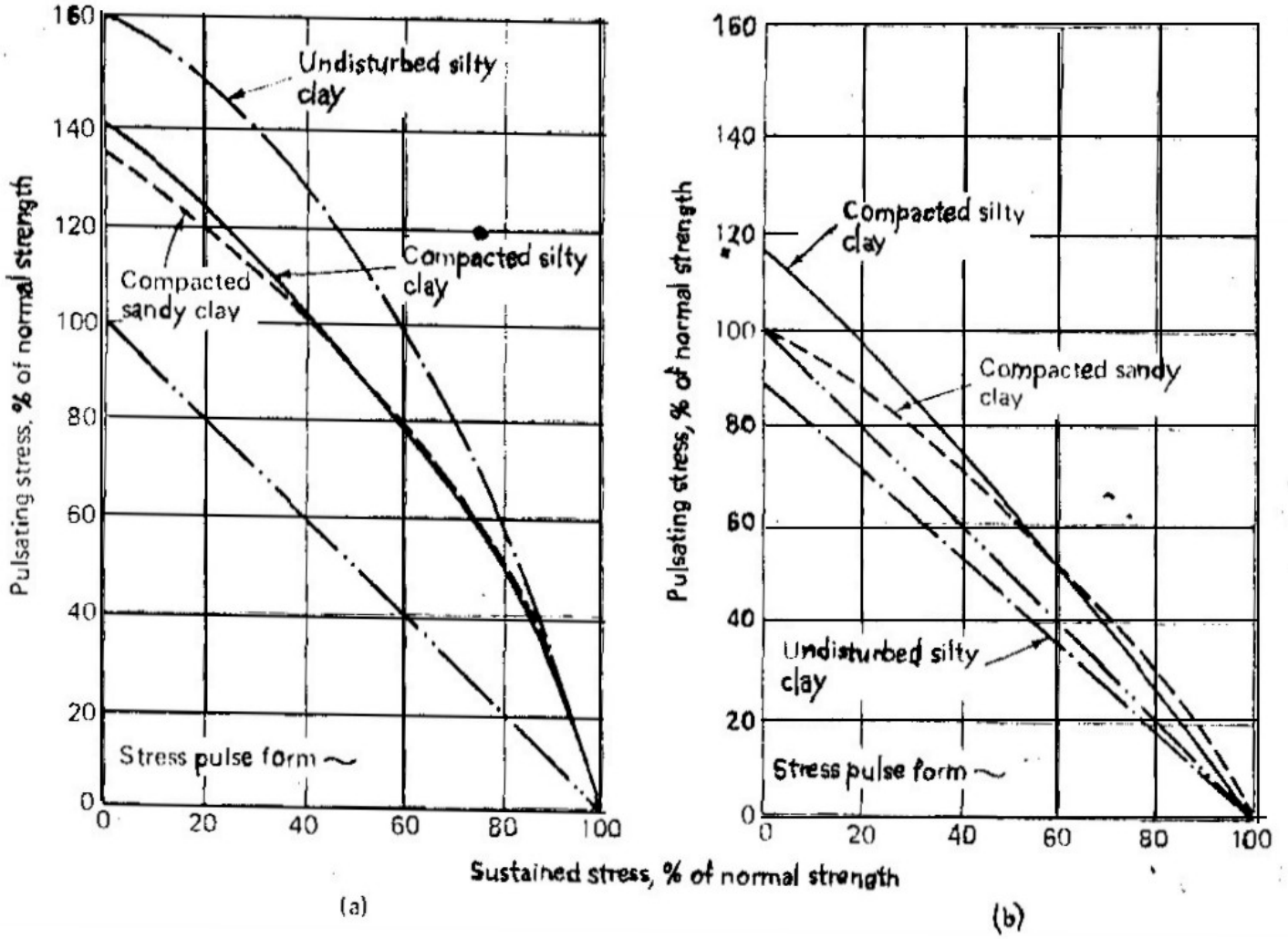

Figure 4.18 Comparison of stress conditions causing failure for different soils. (*a*) 1 pulse. (*b*) 30 pulses. *(After Seed and Chan, 1966.)*

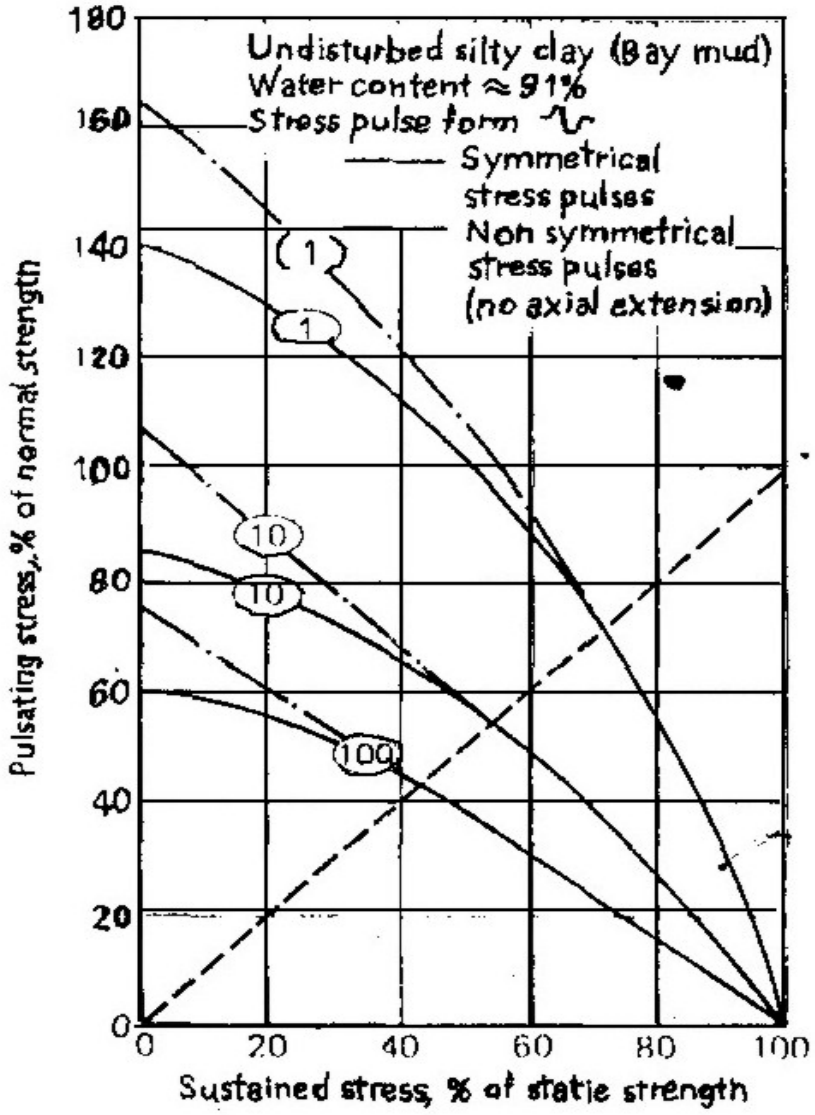

Figure 4.19 Combinations of sustained and pulsating stresses causing failure one and two directional loading in San Francisco Bay mud. (After Seed and Chan, 1966.)

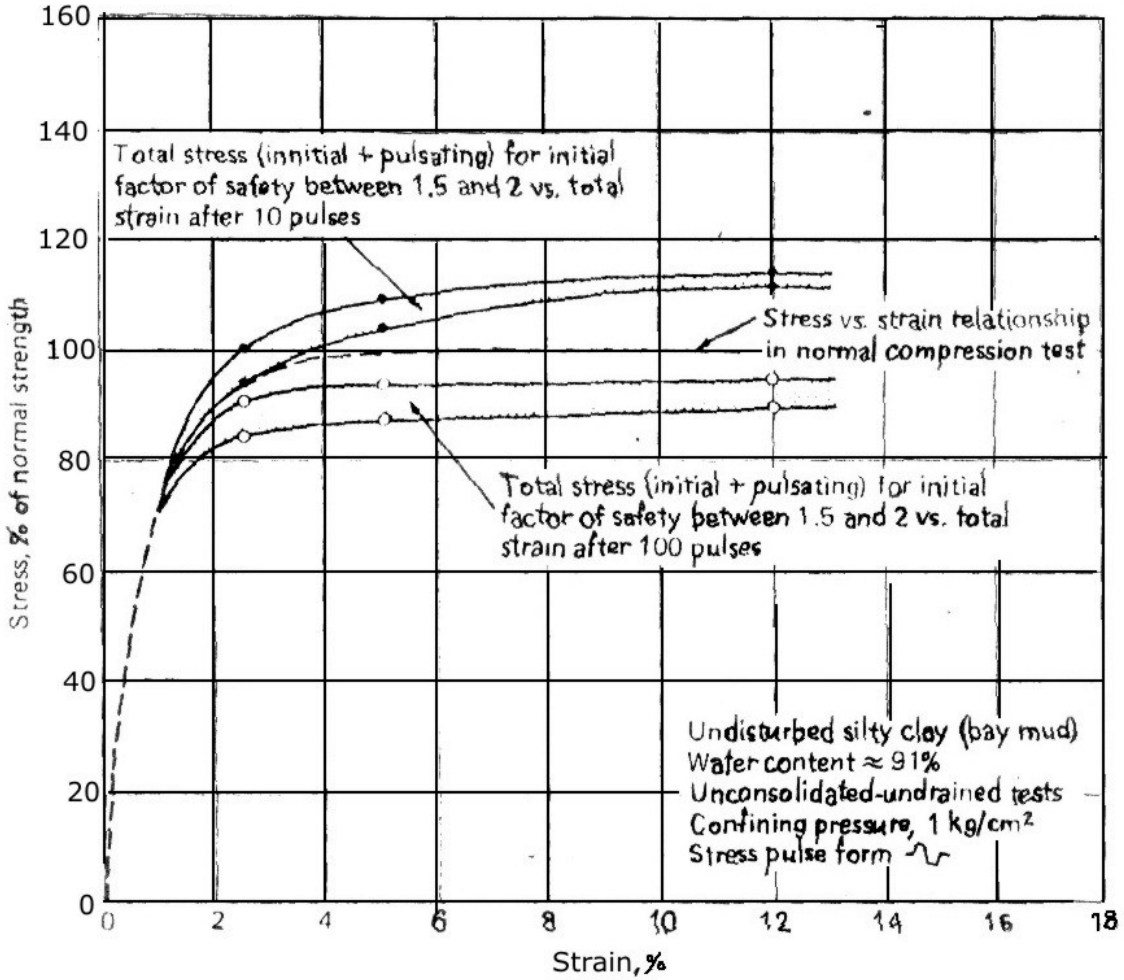

Figure 4.20 Relatioship between total stress and total strain under pulsating load conditions in San Francisco Bay mud. (After Seed and Chan, 1966.)

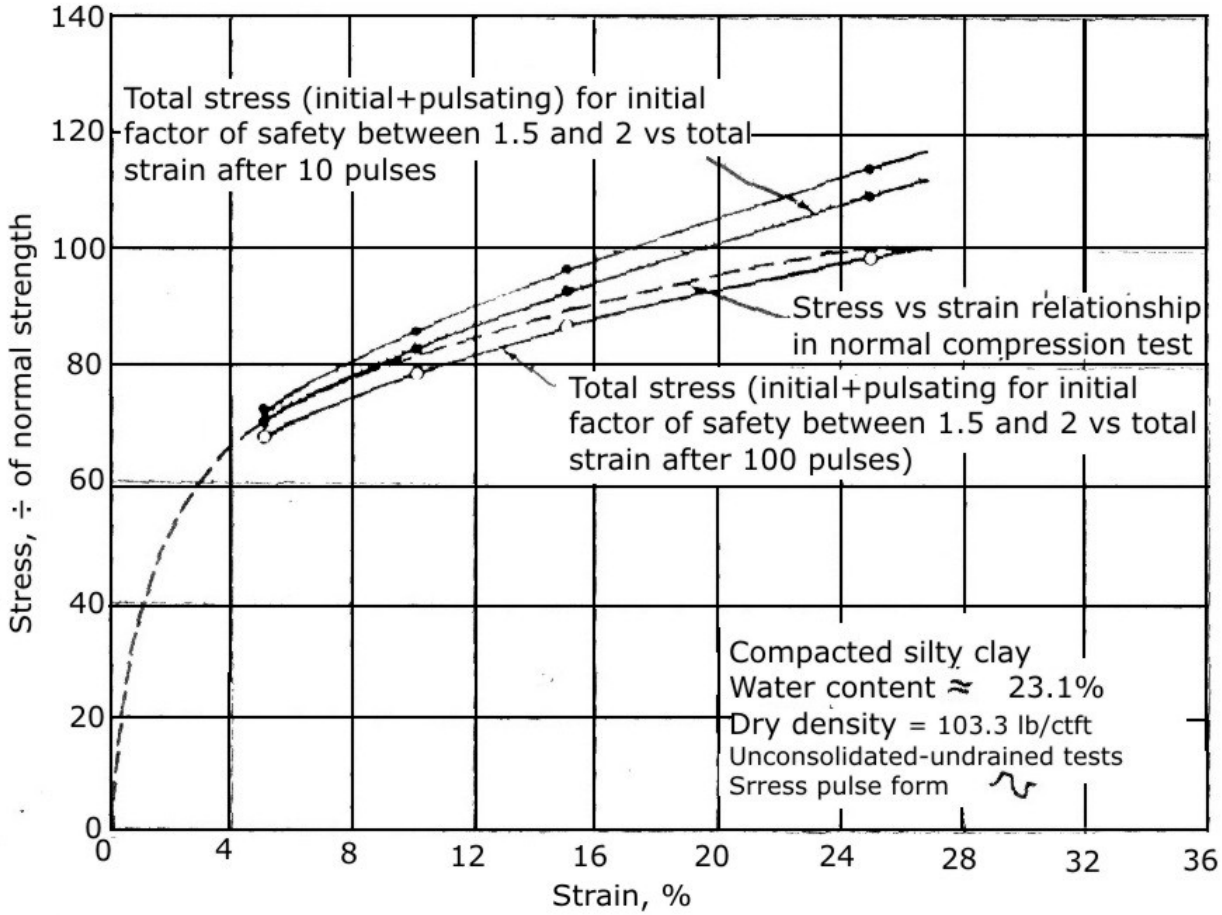

Figure 4.21 Relationship between total stress and total strain under pulsating load conditions in Vicksburg silty clay. (After Seed and Chan, 1966.)

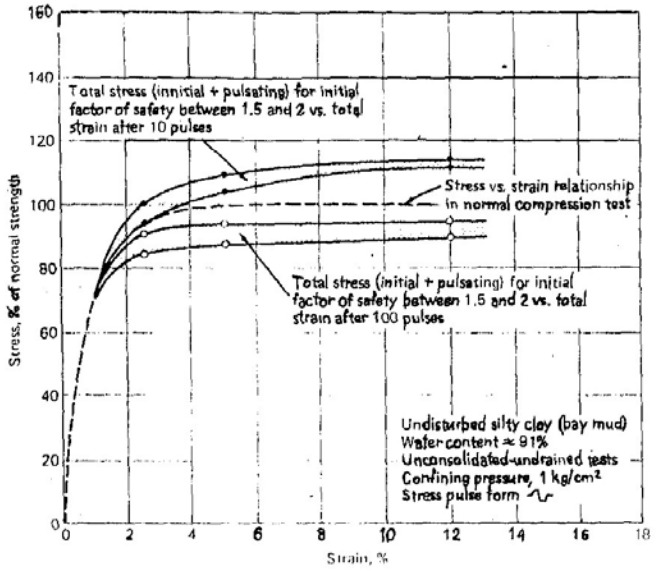

Figure 4.20 Relationship between total stress and total strain under pulsating load conditions in San Francisco Bay mud. *(After Seed and Chan, 1966.)*

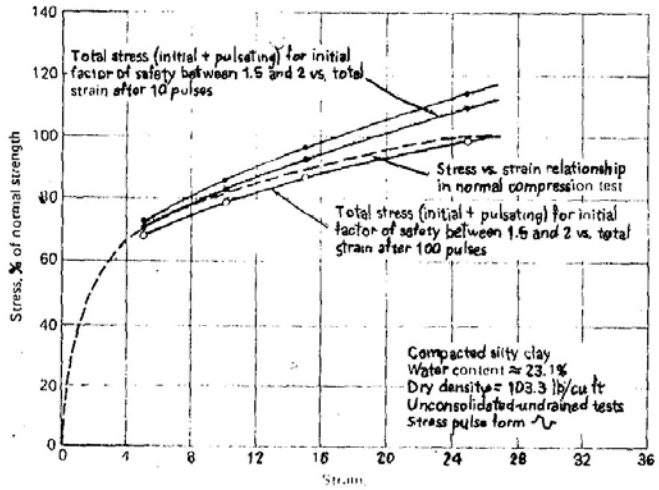

Figure 4.21 Relationship between total stress and total strain under pulsating load conditions in Vicksburg silty clay. *(After Seed and Chan, 1966.)*

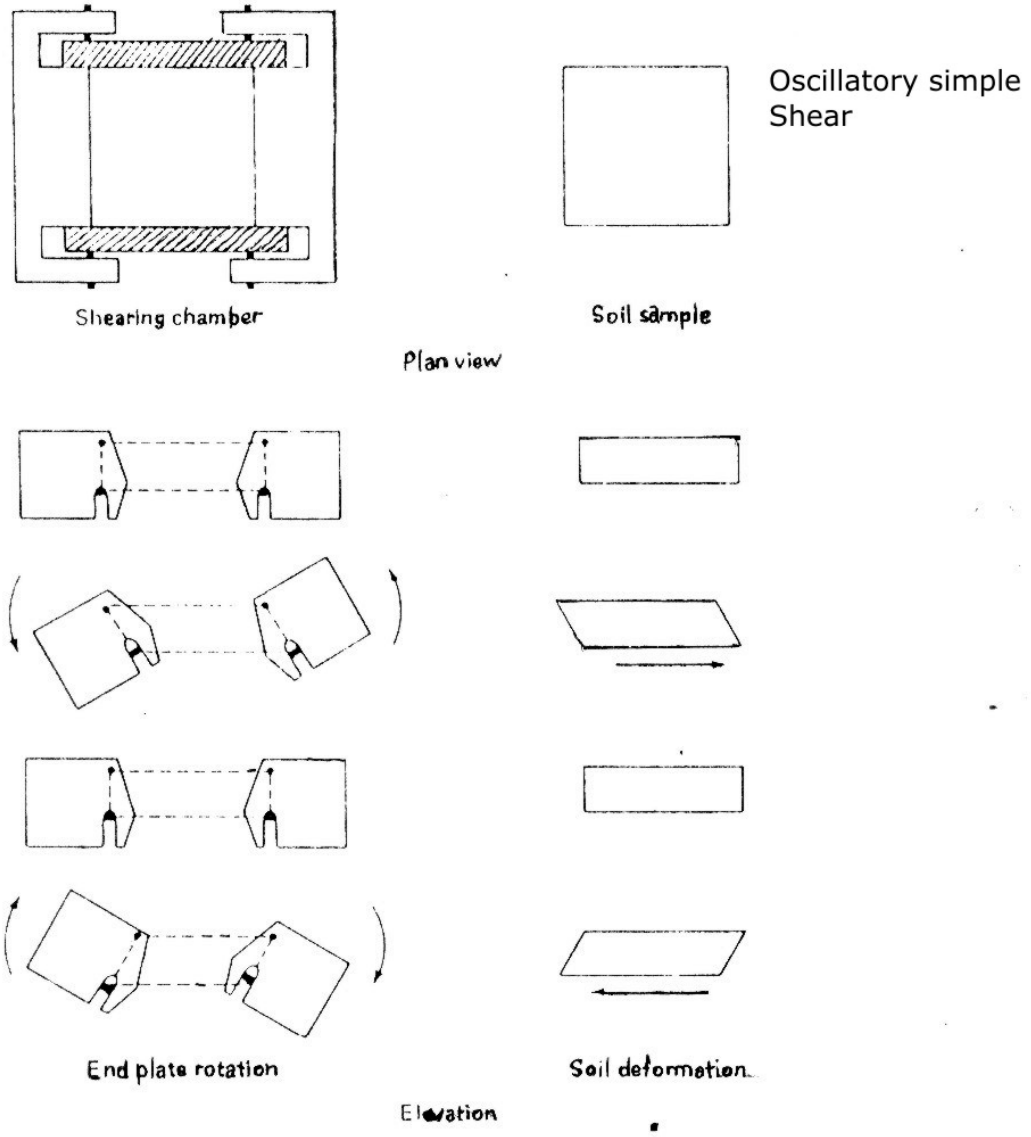

Figure 4.24 Schematic diagram illustrating rotation of hinged end plates and soil deformation in oscillatory simple shear. (After Peacock and Seed, 1968.)

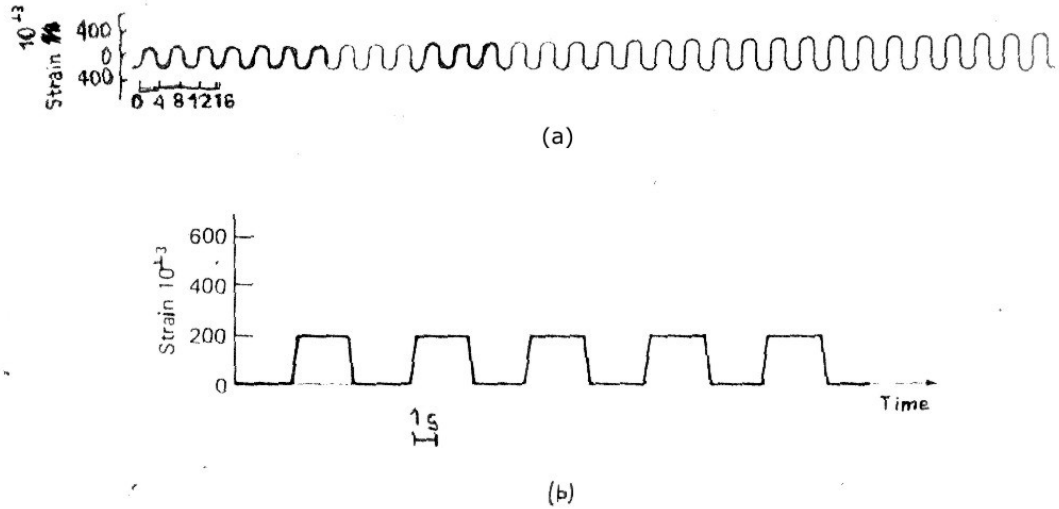

Figure 4.25 Timewise record of strain in (*a*) load gauge (*b*) displacement gauge. (*After Prakash, Nandkumaran, and Joshi, 1973.*)

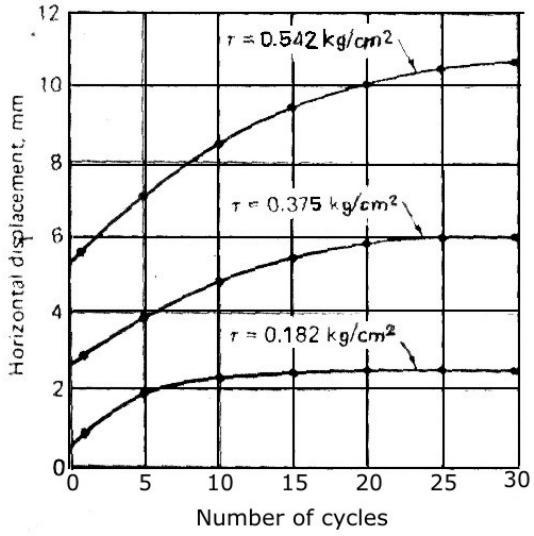

Figure 4.26 Number of cycles vs. horizontal displacement in oscillatory simple shear in sample no. 1 ($\sigma_n = 0.292$ kg/cm², $f = 0.175$ Hz.) (After Prakash. Nandkumaran, and Bansal, 1974.)

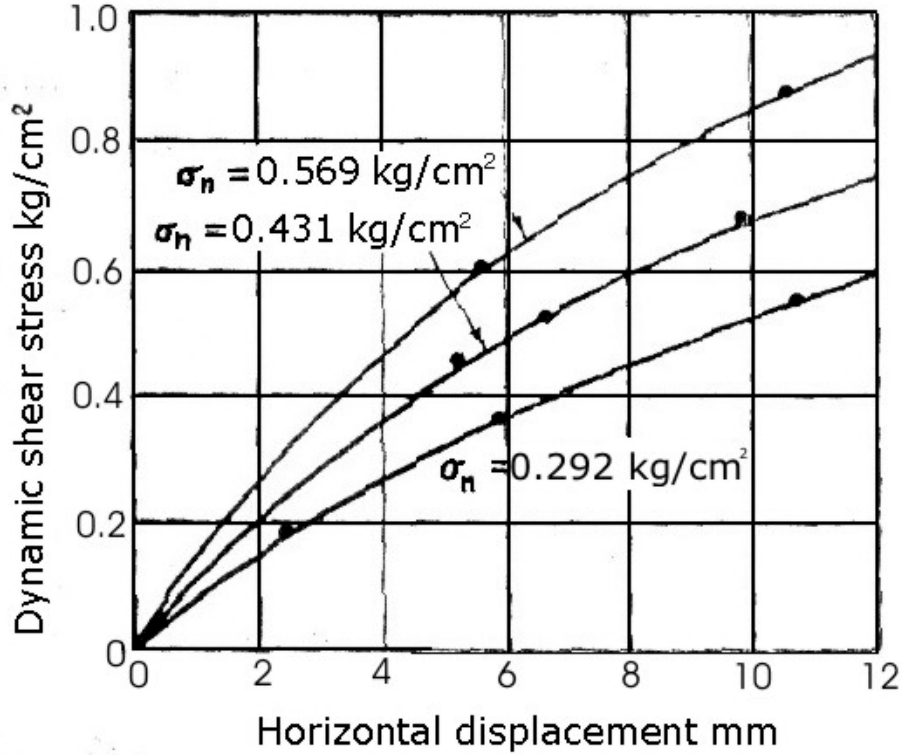

Figure 4.27 Dynamic shear stress vs. horizontal displacement in 30 cycles in sample no. 1. (After Prakash, Nandkumaran, and Bansal, 1974.)

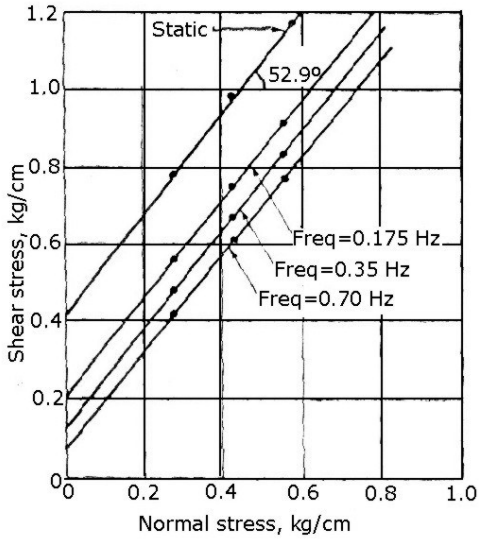

(a)

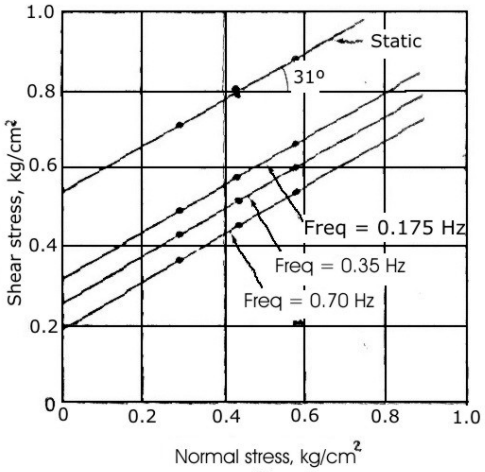

(b)

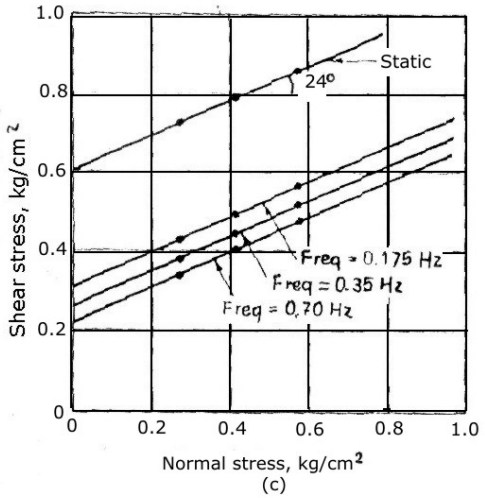

(c)

Figure 4.28 Mohr envelopes for static and dynamic stresses. (*a*) SM (*b*) CL (c) CH (*After Prakash, Nandkumaran, and Bansal, 1974.*)

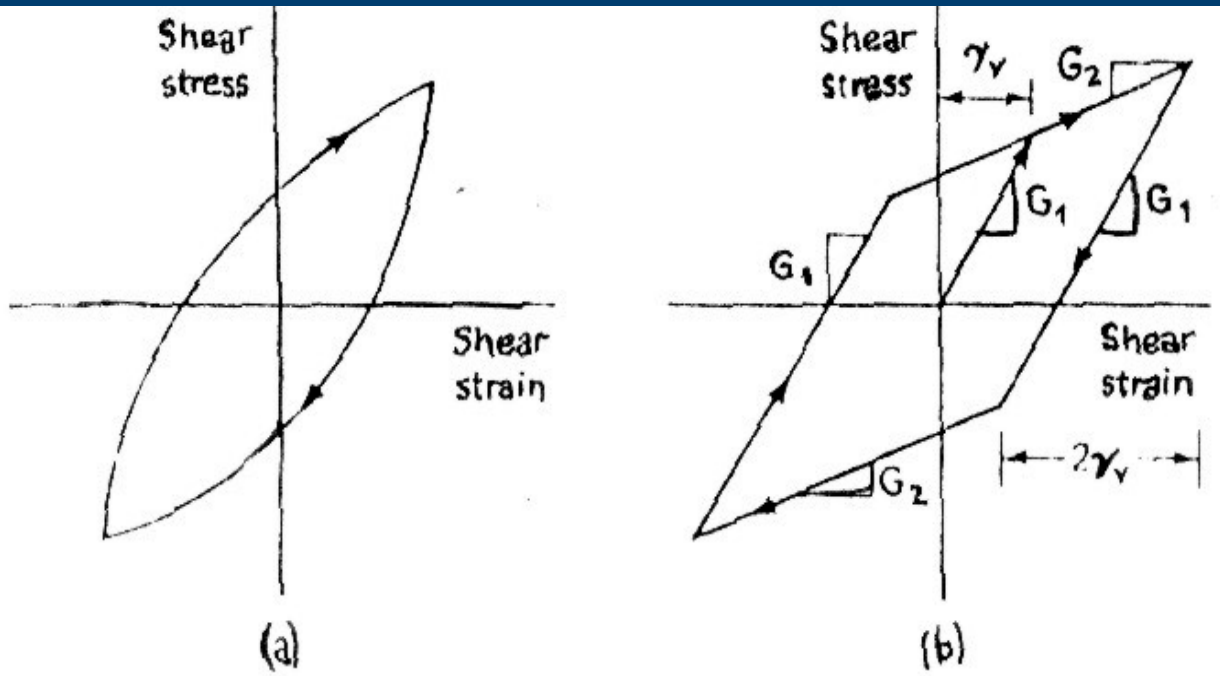

Figure 4.29 (*a*) Stress-strain curve of a soil and (*b*) bilinear model. (*After Thiers and Seed, 1968.*)

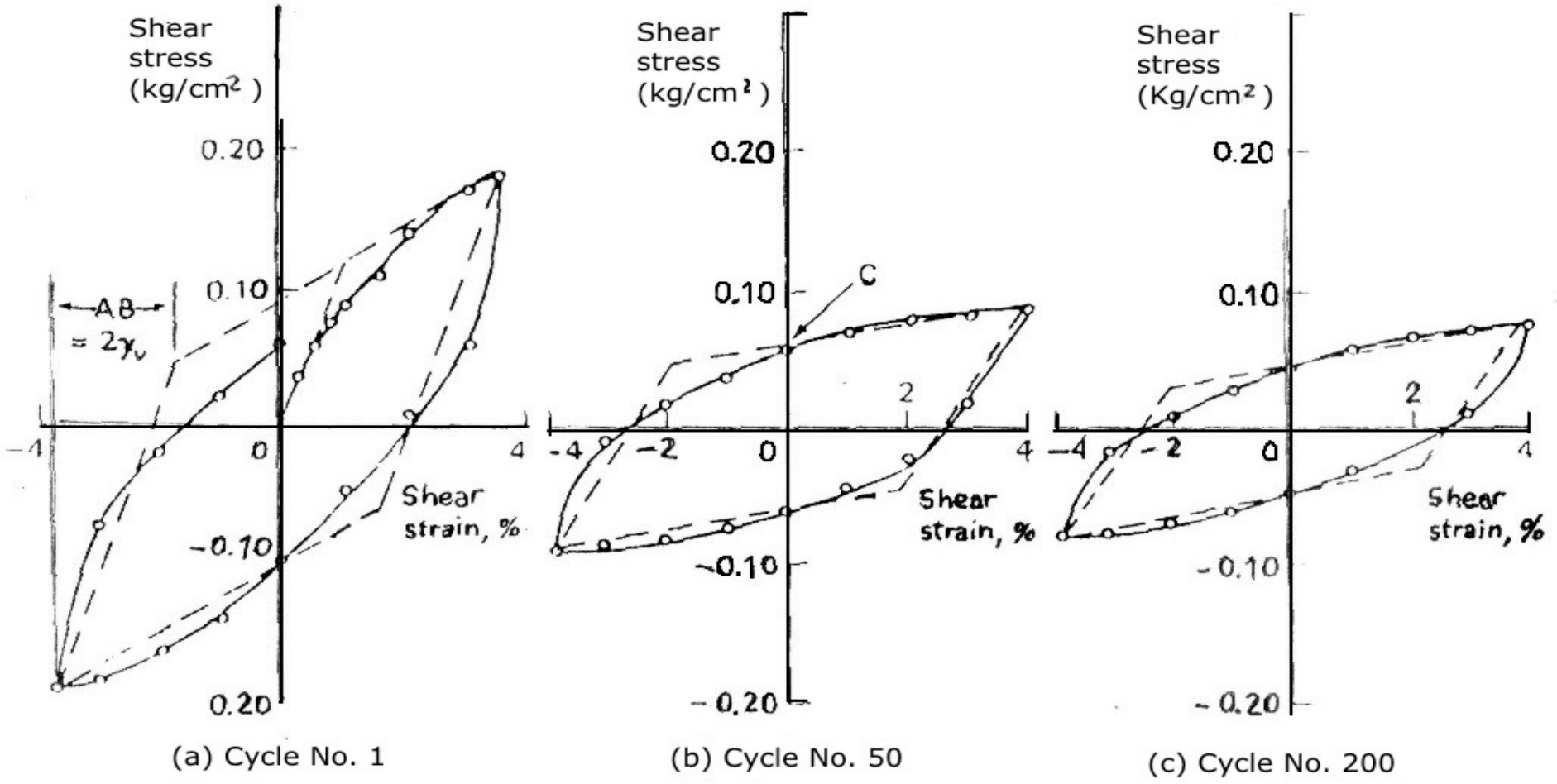

Figure 4.30 Stress-strain curves and bilinear models in San Francisco Bay mud (a) Cycle no. 1. (b) Cycle no. 50. (c) Cycle no. 200. (After Thiears and Seed, 1968.)

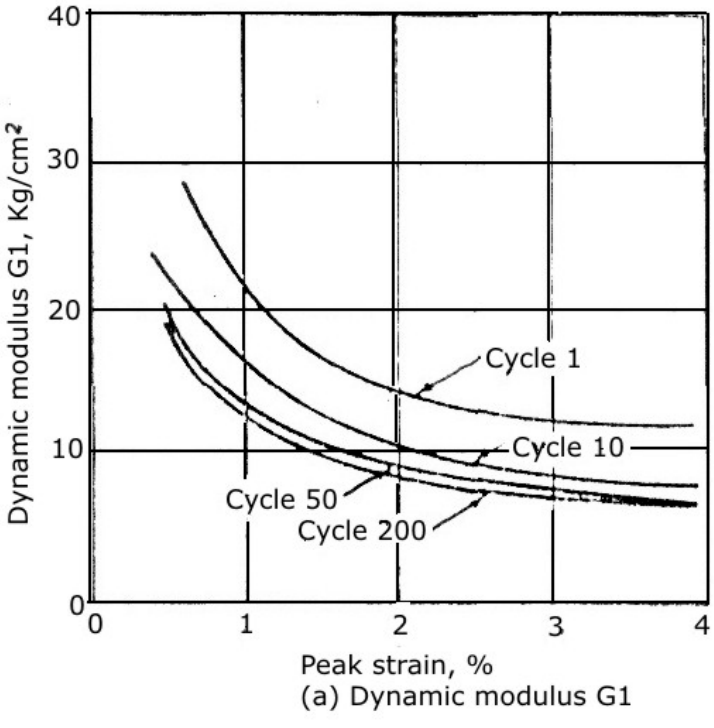

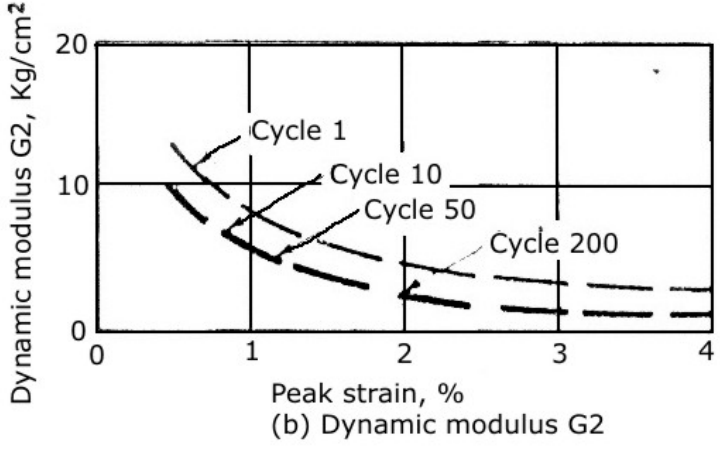

Figure 4.31 Effect of cycling loading on dynamic moduli. (a) Dynamic modulus G1 (b) Dynamic modulus G2. (After Thiers and Seed, 1968.)

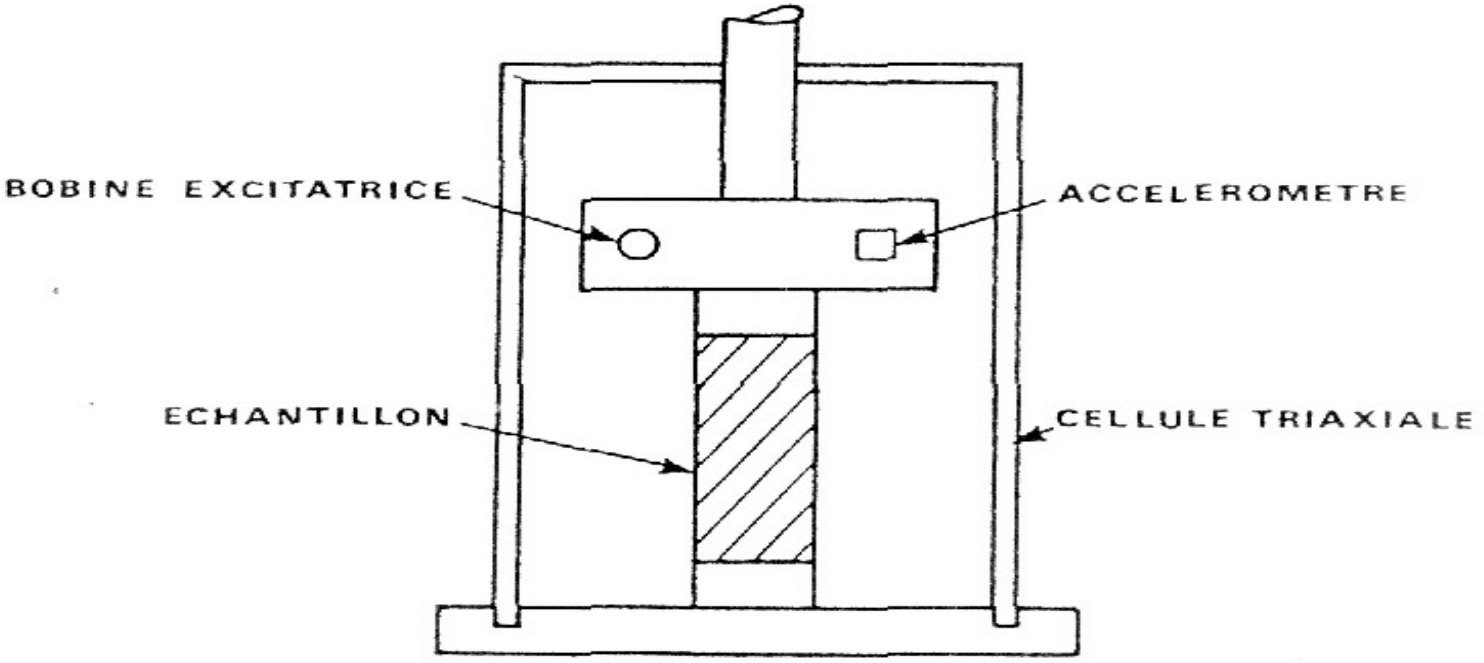

Figure 11 Schéma de l'appareil de colonne résonnante

$v_s = \lambda * fs$. In resonance: $\lambda = 4*L \rightarrow v_s = \lambda * fs = (G/\gamma)^{1/2}$

$v_p = \lambda * fp$. In resonance: $\lambda = 4*L \rightarrow v_p = \lambda * fp = (E/\gamma)^{1/2}$

$$E = G/[2*(1+\nu)]$$

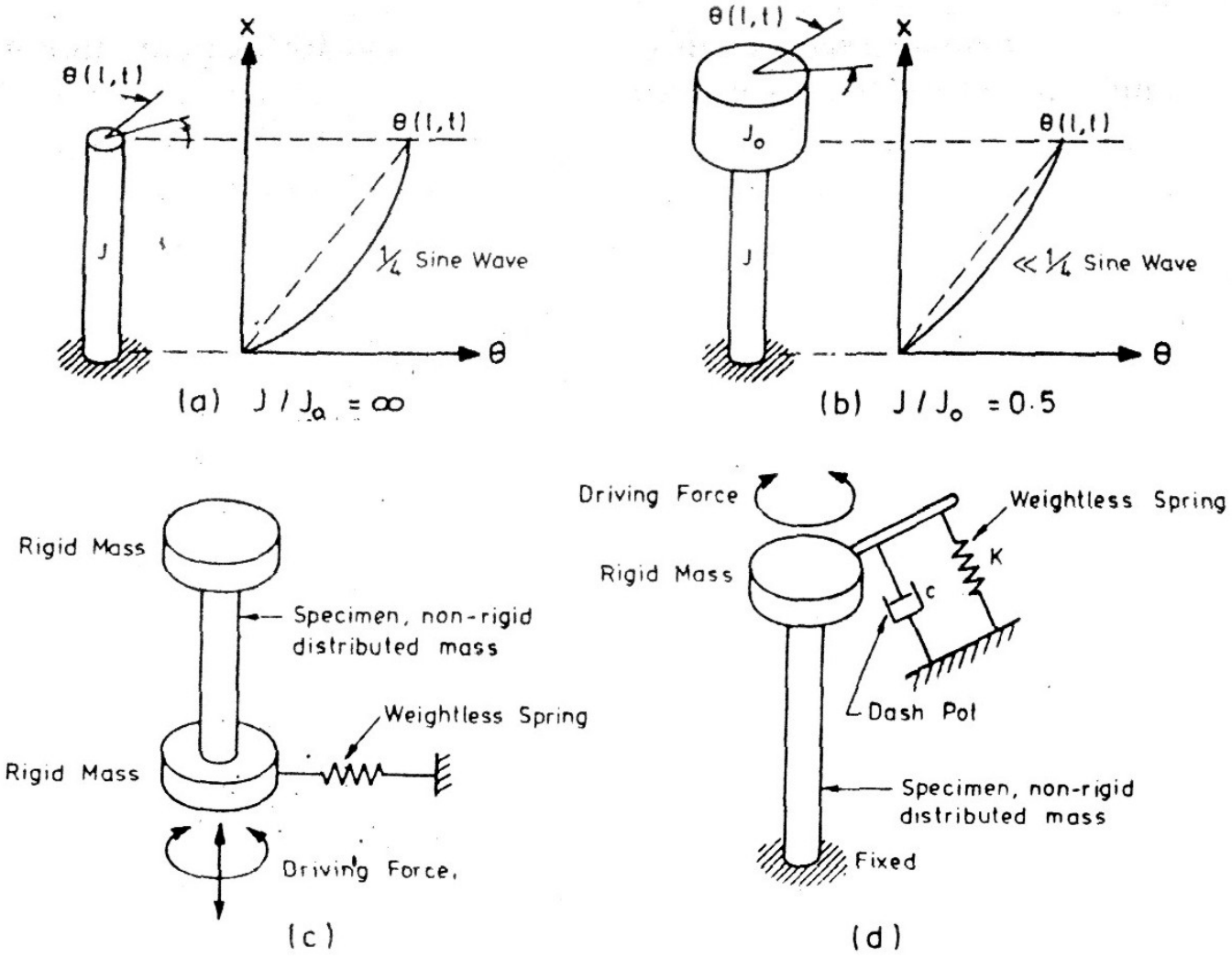

Figure 9.8. Schematic of resonant column end conditions (after Hardin 1965, 1970, and Drnevich 1967; © ASTM, 1916 Race St., Philadelphia, PA 19103; reprinted with permission).

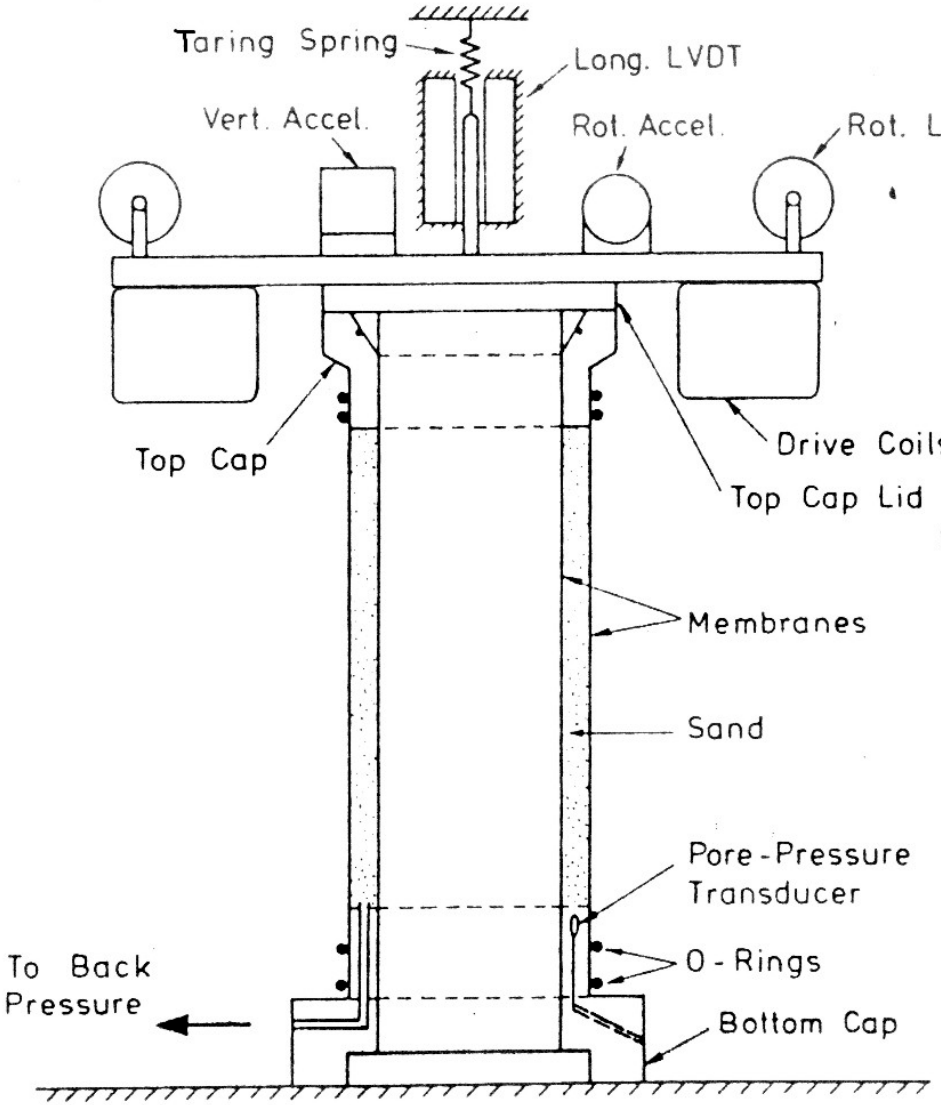

Figure 9.9. Hollow specimen resonant column and torsional shear apparatus (after Drnevich 1972; reprinted by permission of the American Society of Civil Engineers).

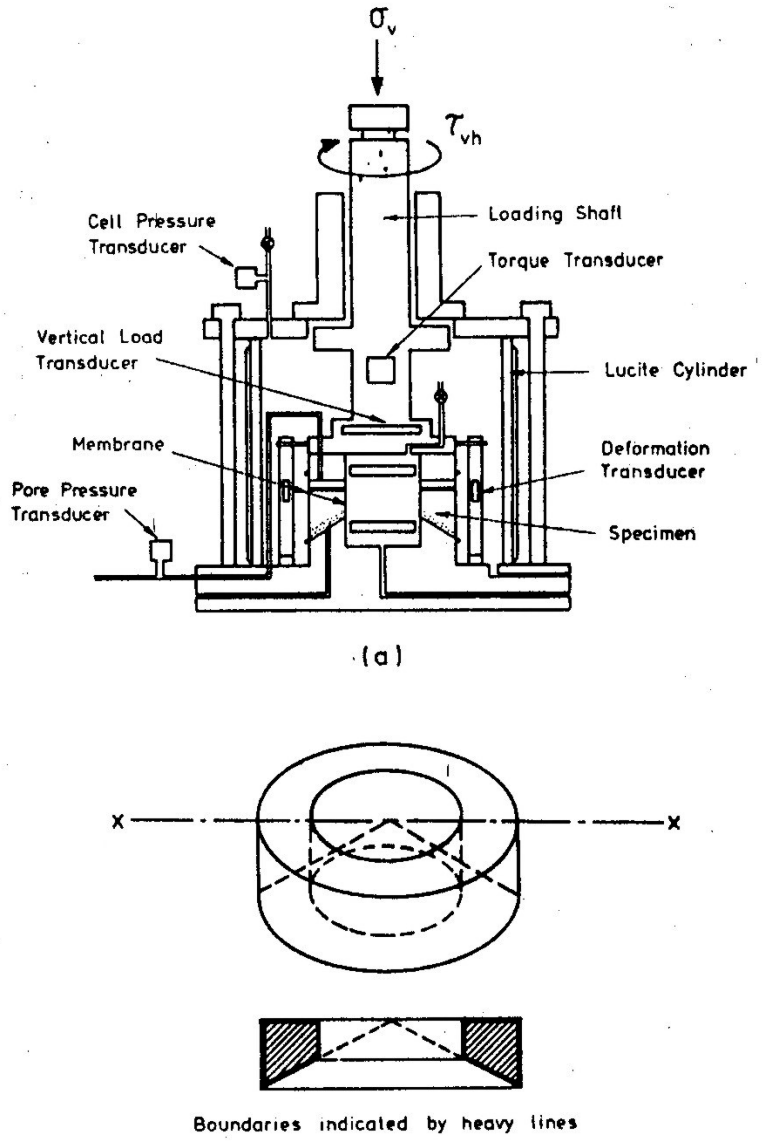

Figure 9.17 Cyclic torsional simple shear apparatus and cross-section for short specimen

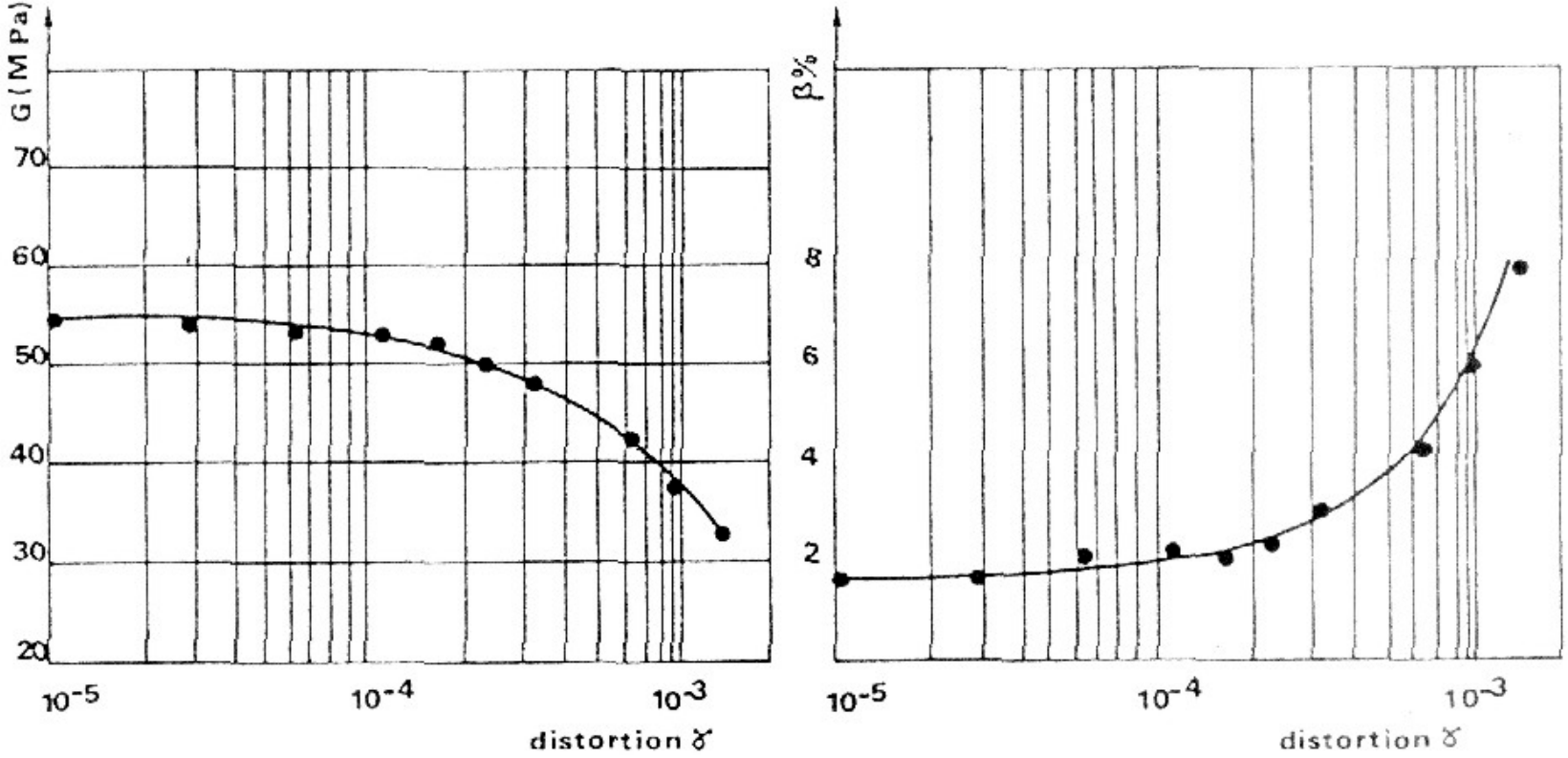

Figure 13 Résultat d'un essai de colonne résonnante

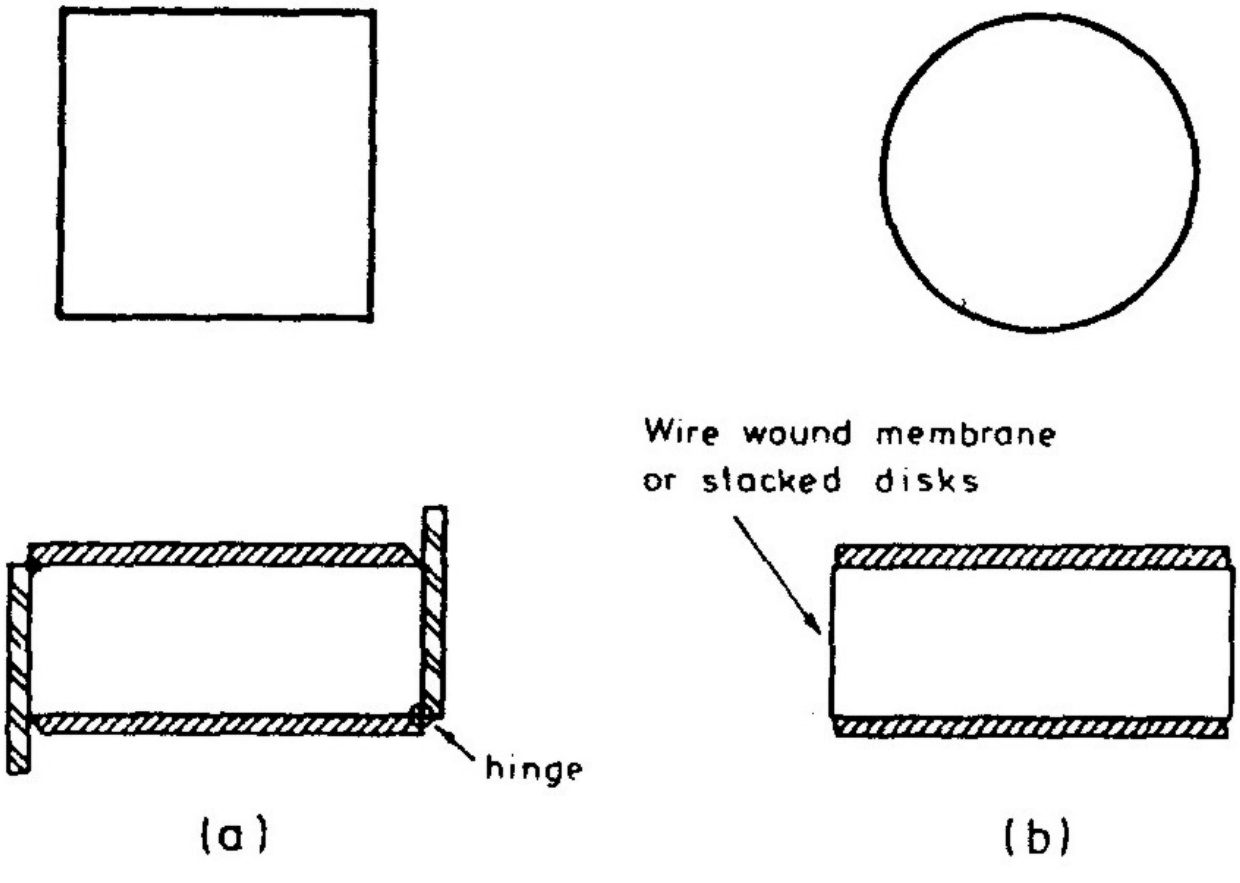

Figure 9.15. Schematic arrangement of (a) Cambridge and (b) NGI/SGI simple shear apparatus.

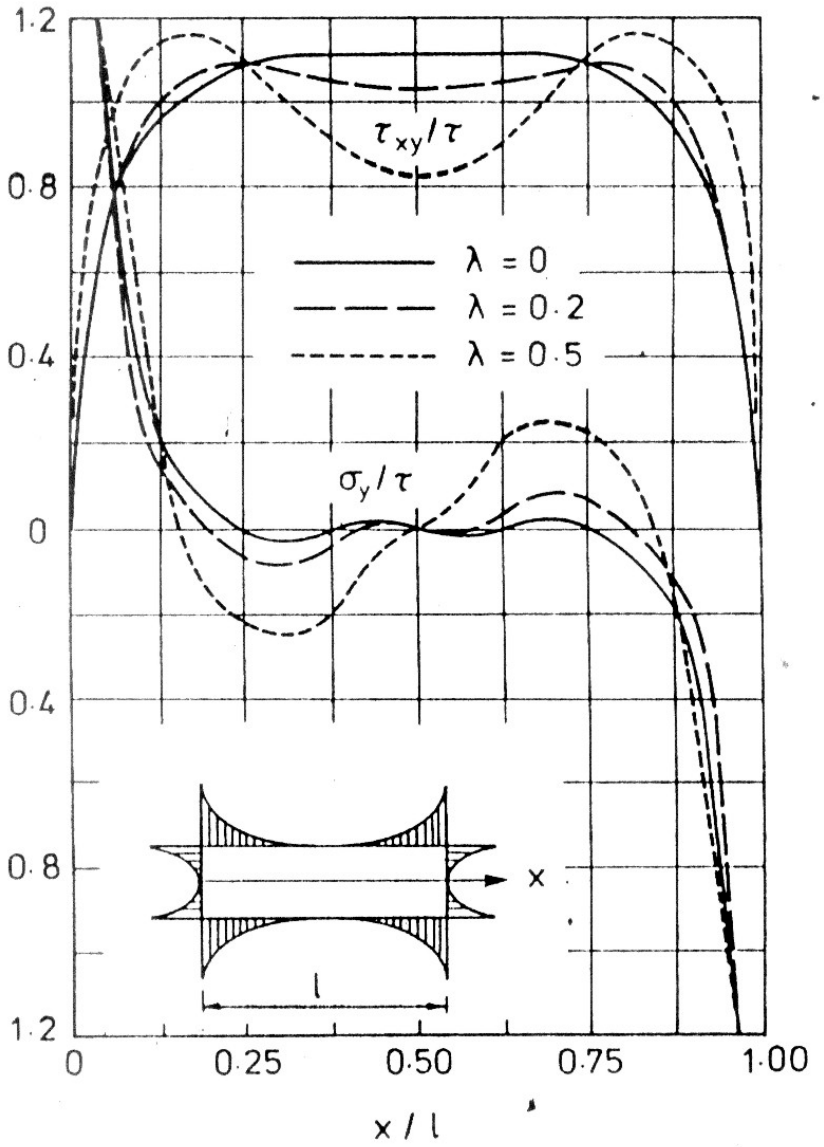

Figure 9.16. Stresses on the upper and lower faces of a simple shear specimen (Cambridge Type) (after Prevost & Hoeg 1976).

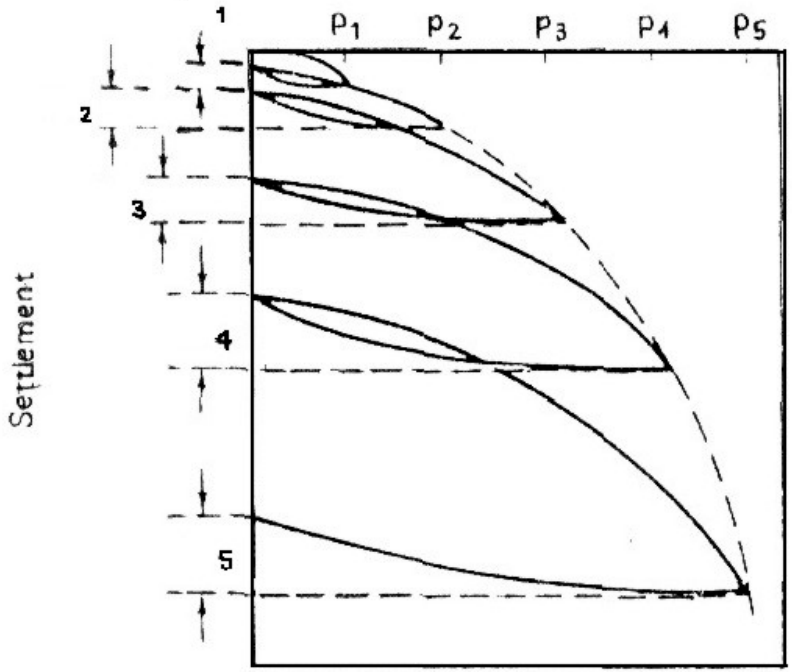

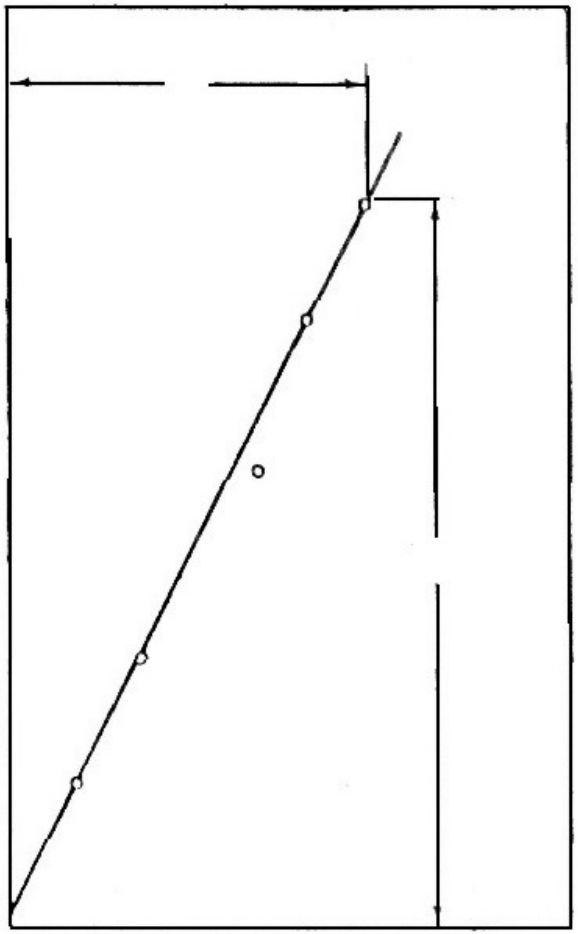

Plate Load Test

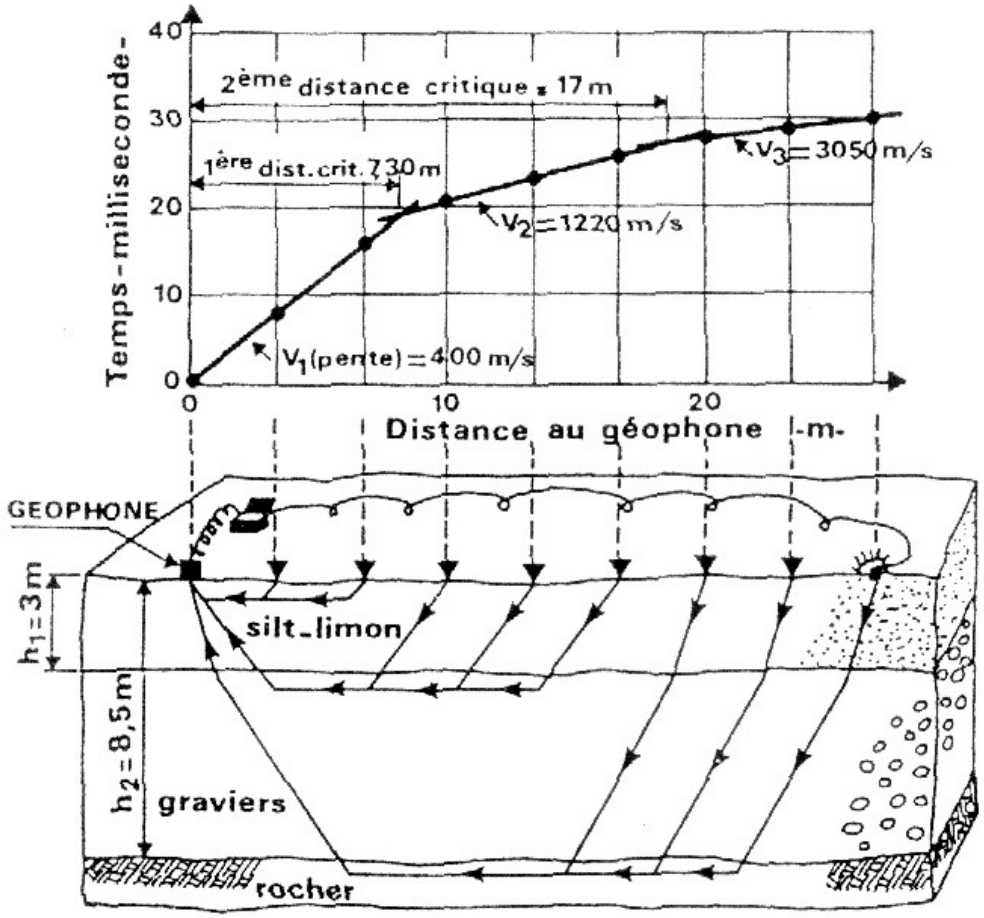

Figure 2 Réfraction sismique

Seismic refraction survey

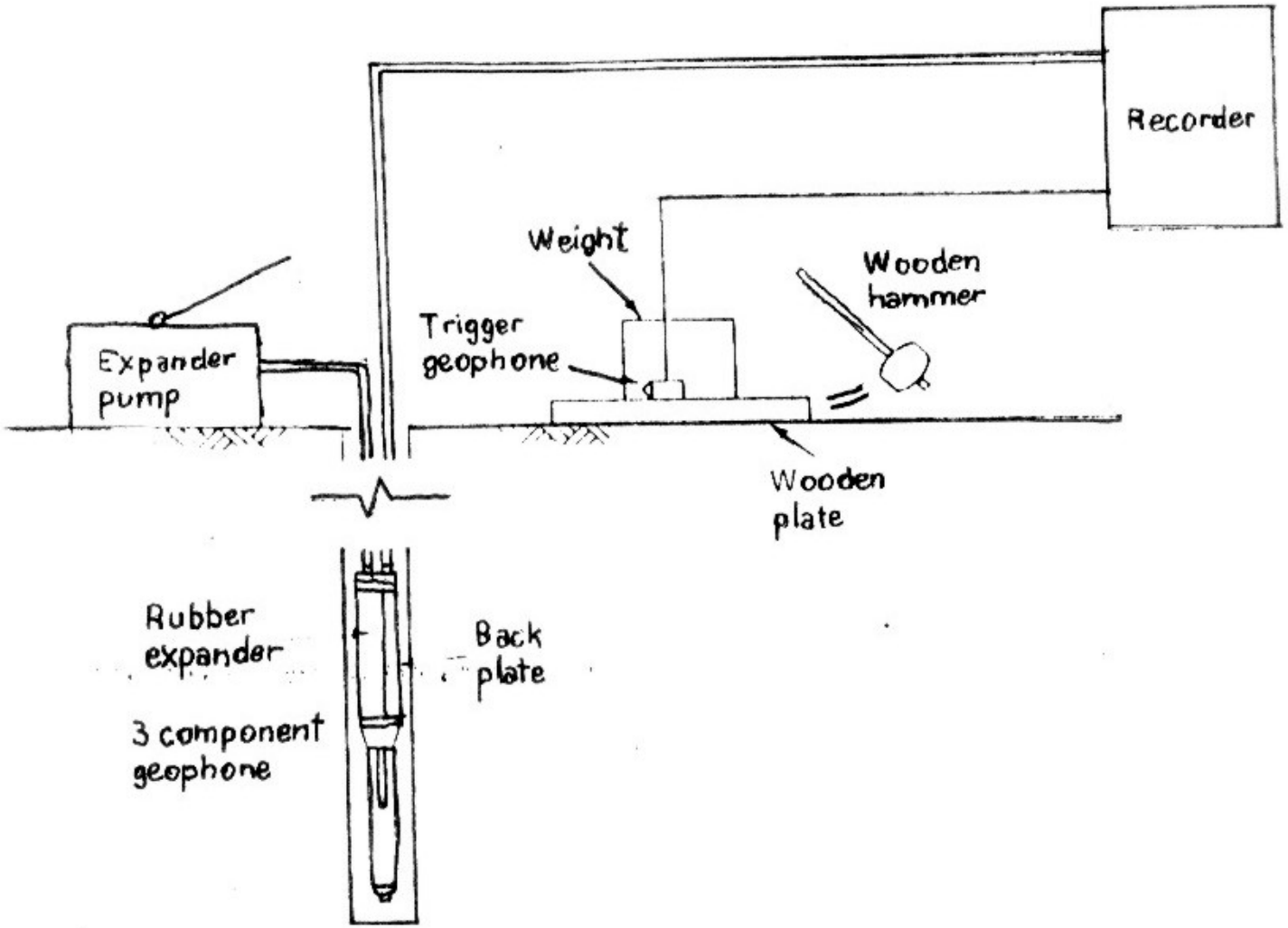

Down – hole test

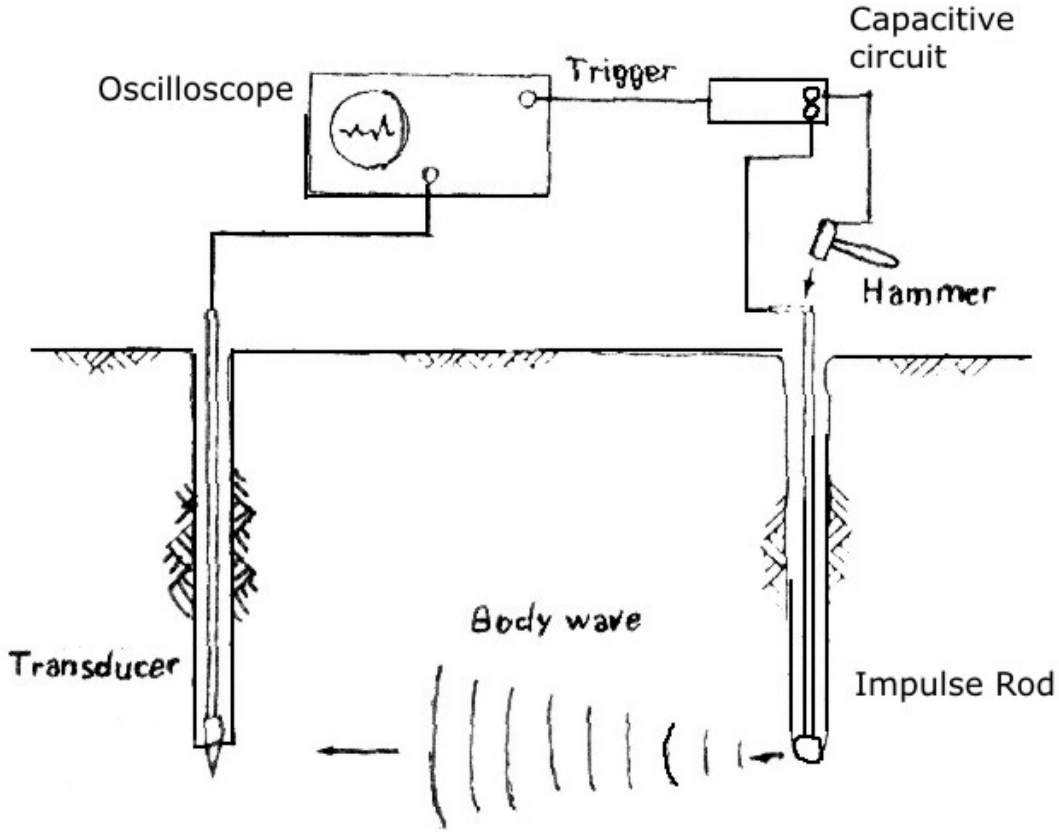

Figure 4.32 Sketch showing cross-bore hole technique for measure-ment of velocity of wave propagation.

Cross – hole test

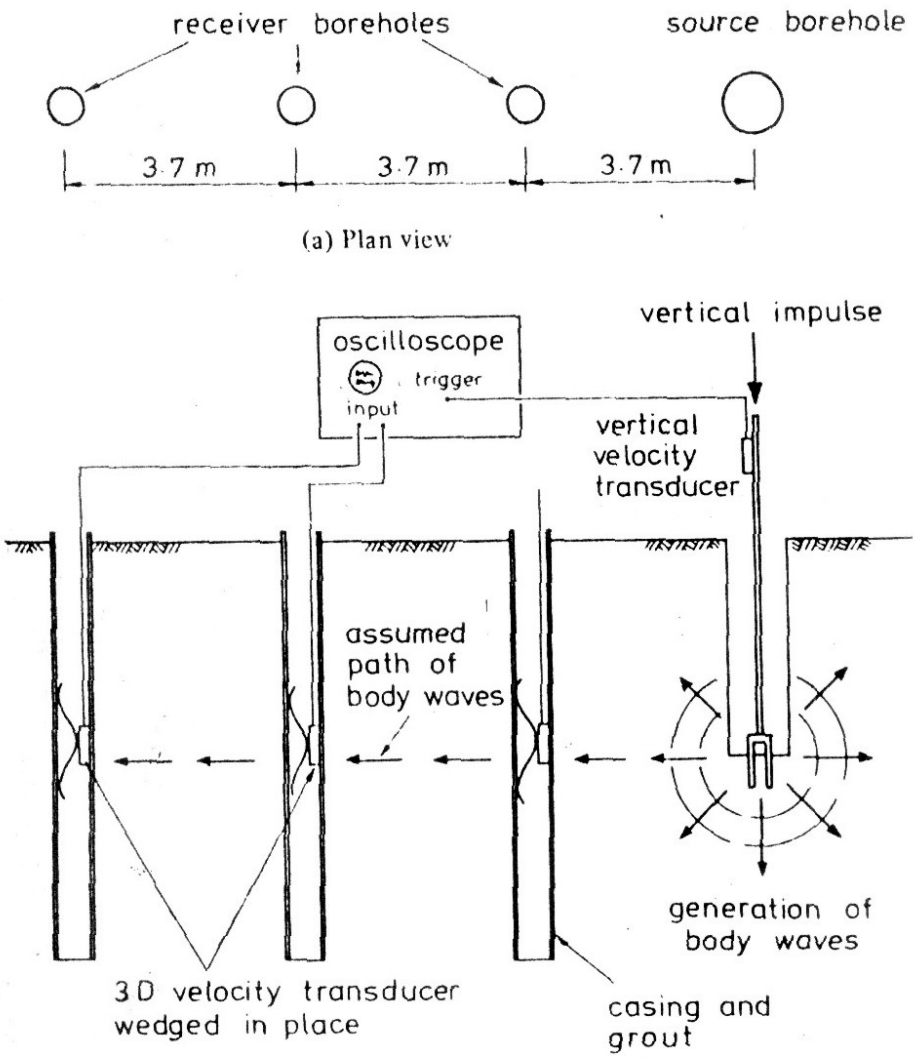

Figure 9.21. Multiple hole seismic cross-hole survey (after Hoar & Stokoe 1978; © ASTM, 1916 Race St., Philadelphia, PA 19103; reprinted with permission).

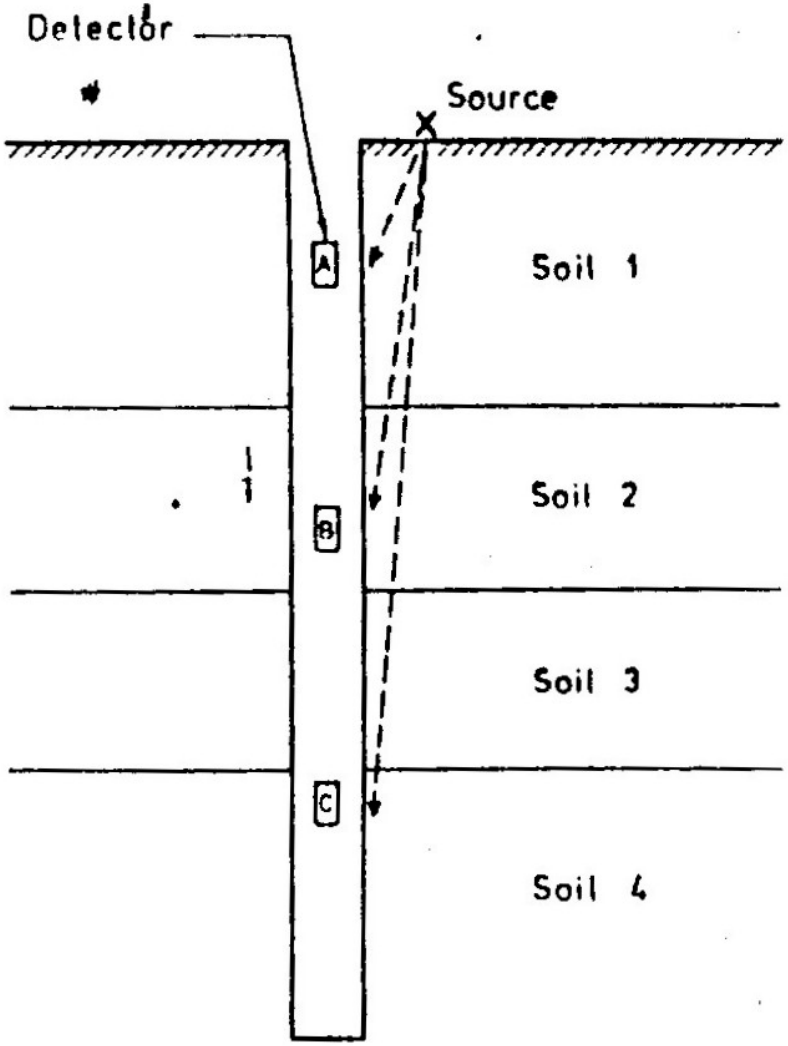

Figure 9.26. Seismic down-hole survey.

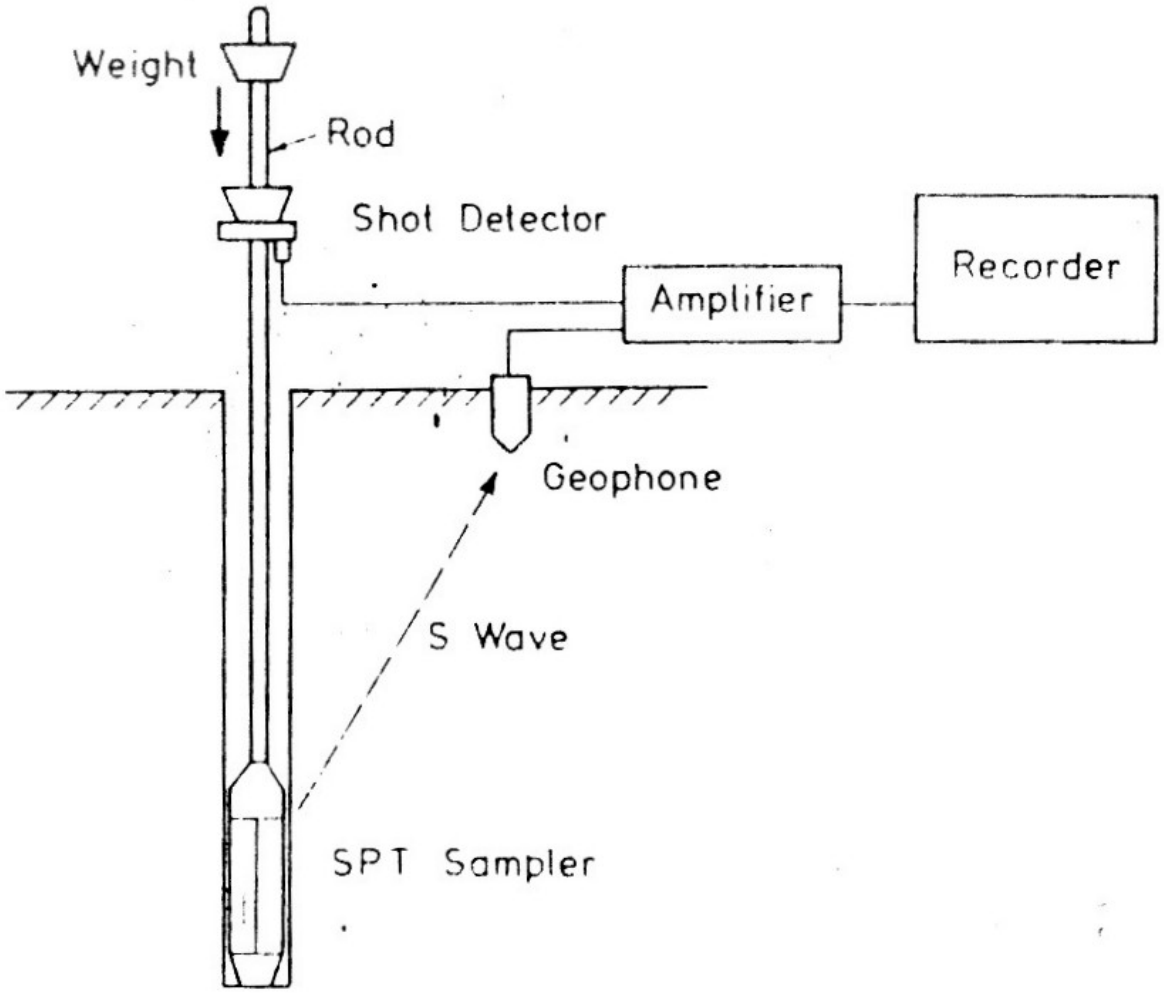

Figure 9.28. Seismic up-hole survey with SPT (after Goto *et al.* 1977).

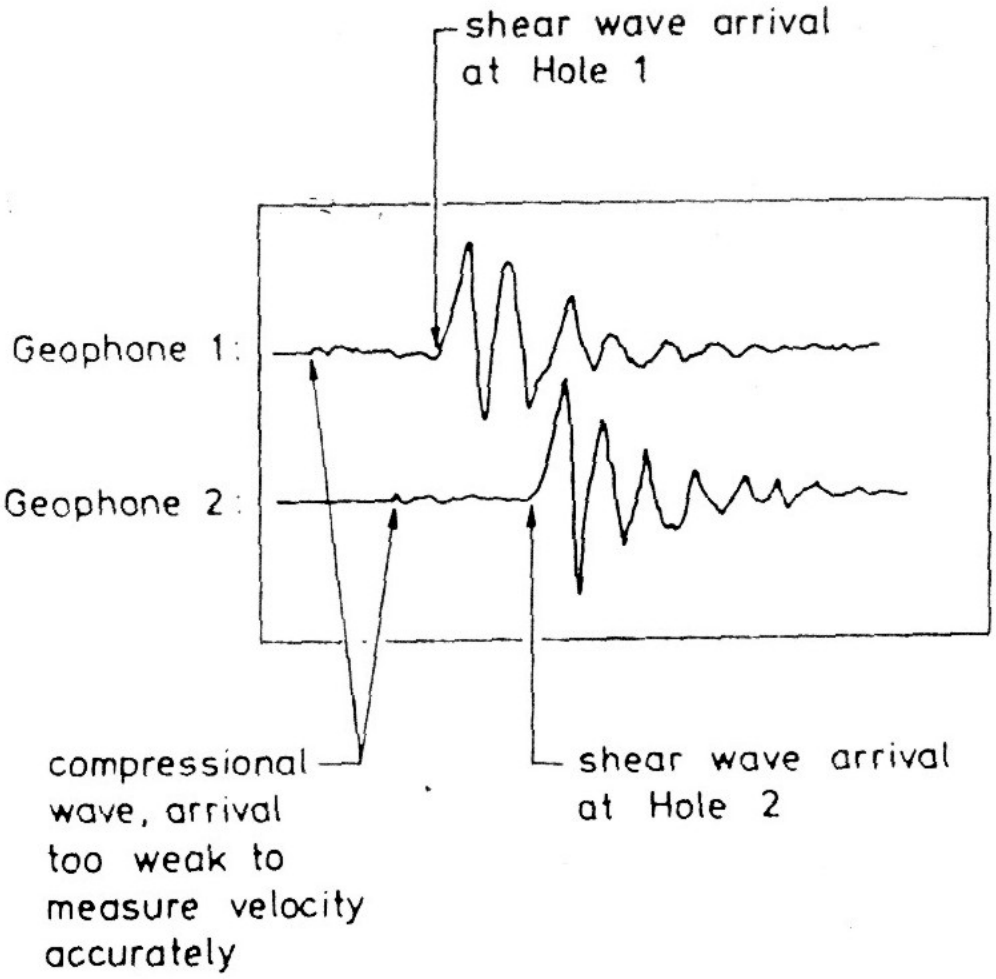

Figure 9.22. Examples of geophone output for seismic cross-hole survey.

Table 4.5 Field techniques for measuring dynamic soil properties*

Field technique	*P*-wave velocity	*S*-wave velocity	Other measurements	Advantages	Disadvantages
Refraction	X	X	Depths and slopes of layers	Reversible polarity Works from surface Samples large zone Preliminary studies	Misses low velocity zones Low strain amplitudes Properties measured are for thin zones near boundaries
Cross-hole	X	X		Known wave path Reversible polarity Works in limited space	Need two or more holes Need to survey holes for verticality
Down-hole of up-hole	X	X		One hole only Reversible polarity Finds low velocity Works in limited space	Measures average velocities Ambient noise near surface Low strain amplitude
Surface		X	Attenuation of *R* wave	Work from surface	Uncertain about effective deep Needs large vibrator
SPT			Empirical correlation with liquefaction	Widely available Widely used in past	Needs "standardization"
Resonant footing			Modulus of near-surface soils	Works from surface	Limited depth of influence

Table 9.11. Field techniques for measuring dynamic soil properties (after Woods 1978; reprinted by permission of the American Society of Civil Engineers).

Field technique	P-wave velocity	S-wave velocity	Other measurements	Advantages	Disadvantages
Refraction	x	x	Depths and slopes of layers	Reversible polarity with SH-SRS Work from surface Samples large zone Preliminary studies	Miss low velocity zones low strain amplitudes Properties measured are for thin zones near boundaries
Cross-hole	x	x	Velocity as function of strain amplitude	Known wave path Reversible polarity Works in limited space Finds low velocity	Need 2 or more holes Holes must be surveyed for verticality. Needs short time interval resolution
(In situ impulse test)	x	x			
Down-hole (up-hole)	x	x		One hole Reversible polarity Finds low velocity	Measure average velocities Ambient noise near surface Low strain amplitude
Surface		x	Attenuation of R-wave	Works in limites space	Uncertain about effective depth
SPT			Empirical correlation with liquefaction	Widely available Widely used in past	Needs large vibrator Needs 'standardization'
Resonant footing			Modulus of near surface soils	Work from surface	Limited depth of influence
CIST	x	x	Constitutive eq.	Wide amplitude range	Very elaborate

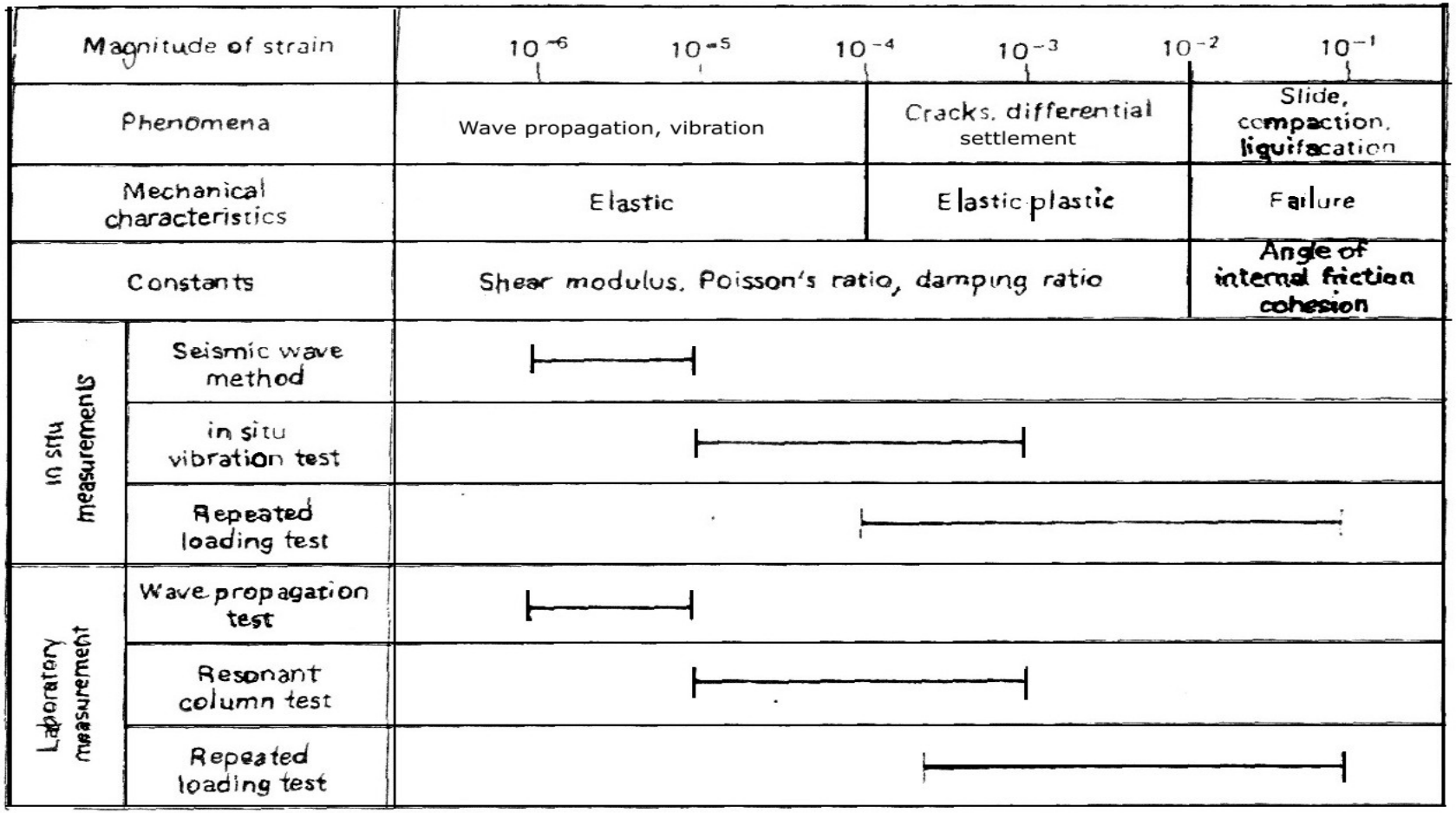

Figure 4.43 Strain level associated with different in situ and laboratory tests. (*After Ishihara, 1971.*)

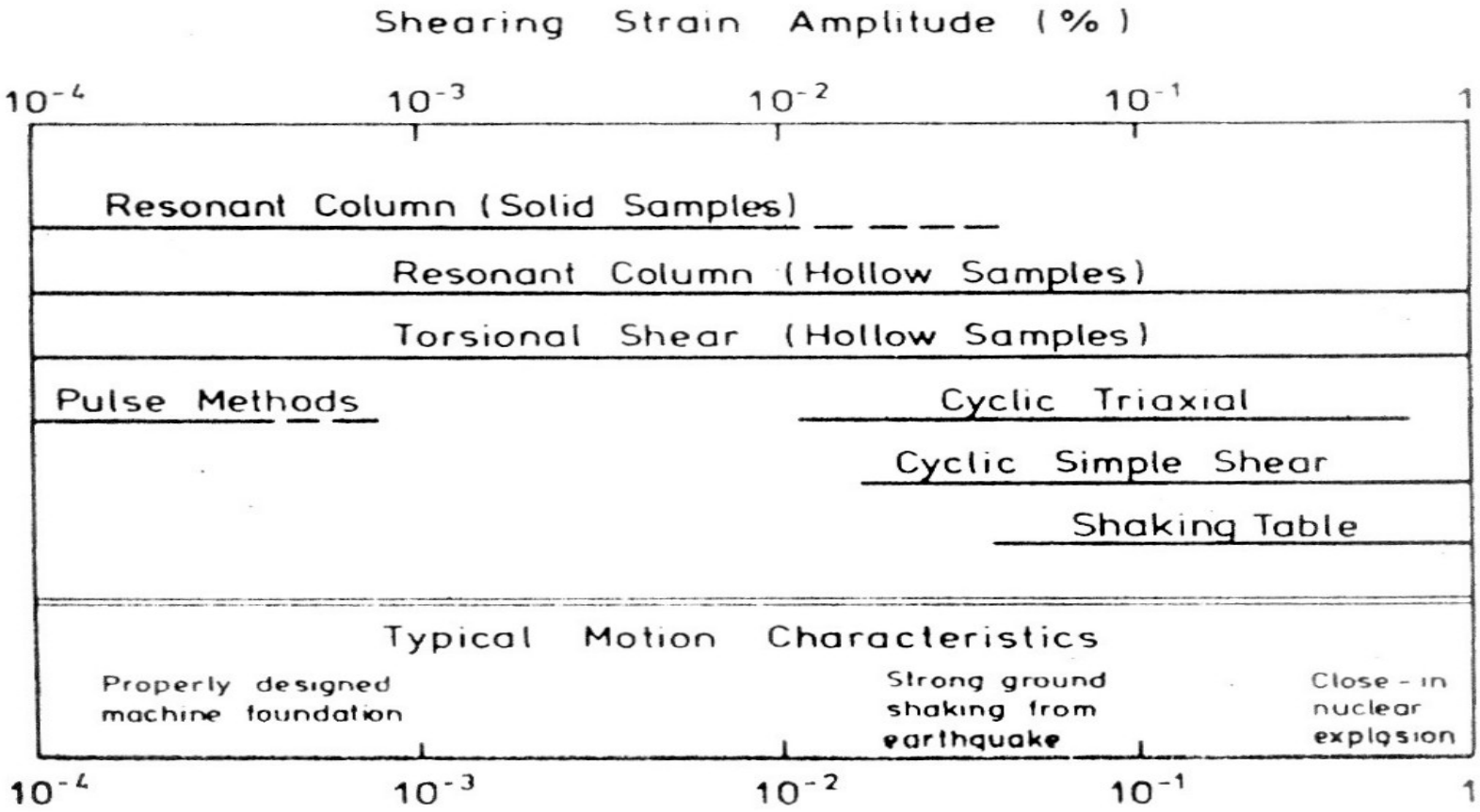

Figure 9.18. Shearing strain amplitude capabilities of laboratory apparatus (after Wood 1978; reprinted by permission of the American Society of Civil Engineers).

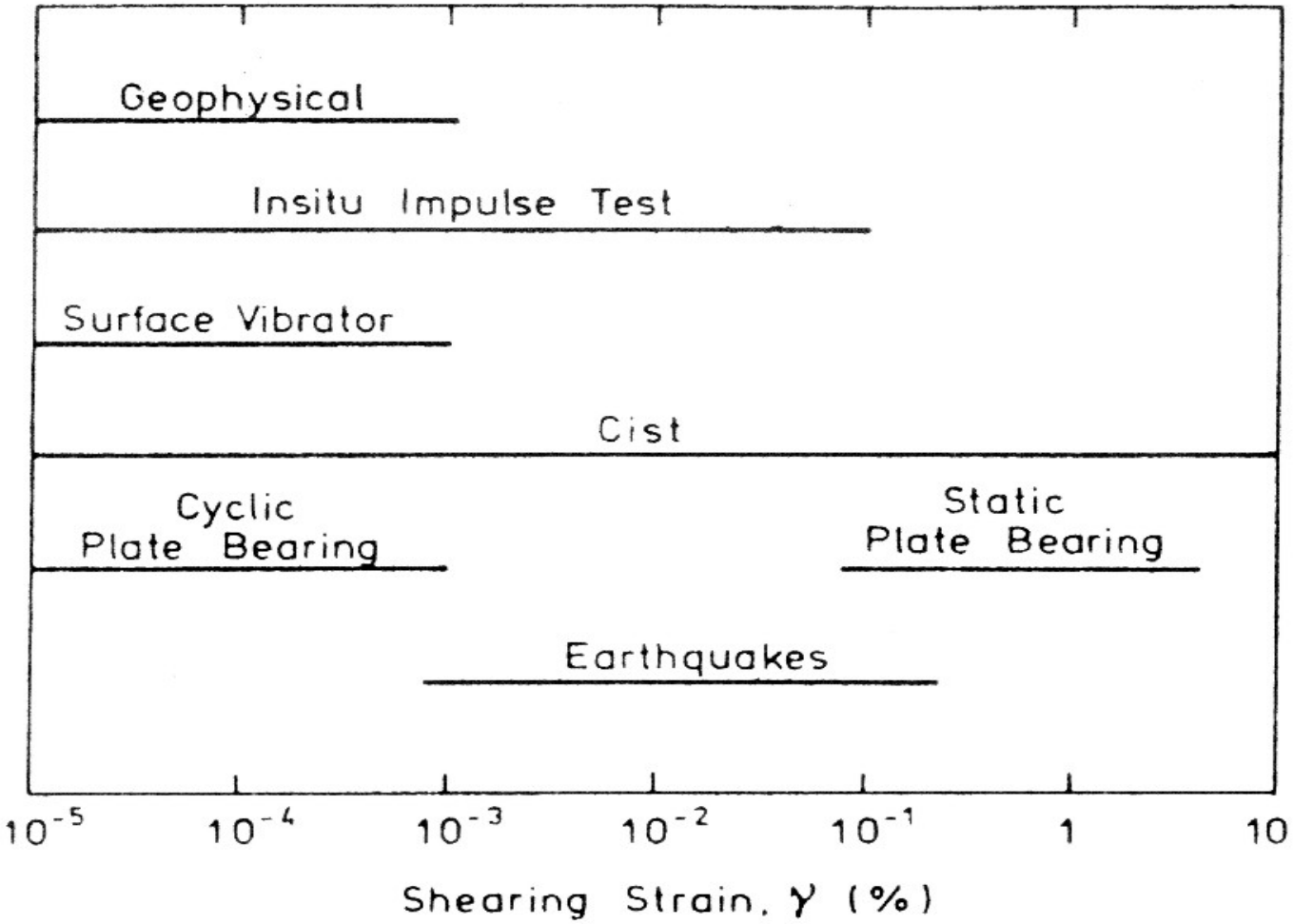

Figure 9.31. Shearing strain amplitude capabilities of field techniques (after Woods 1978; reprinted by permission of the American Society of Civil Engineers).

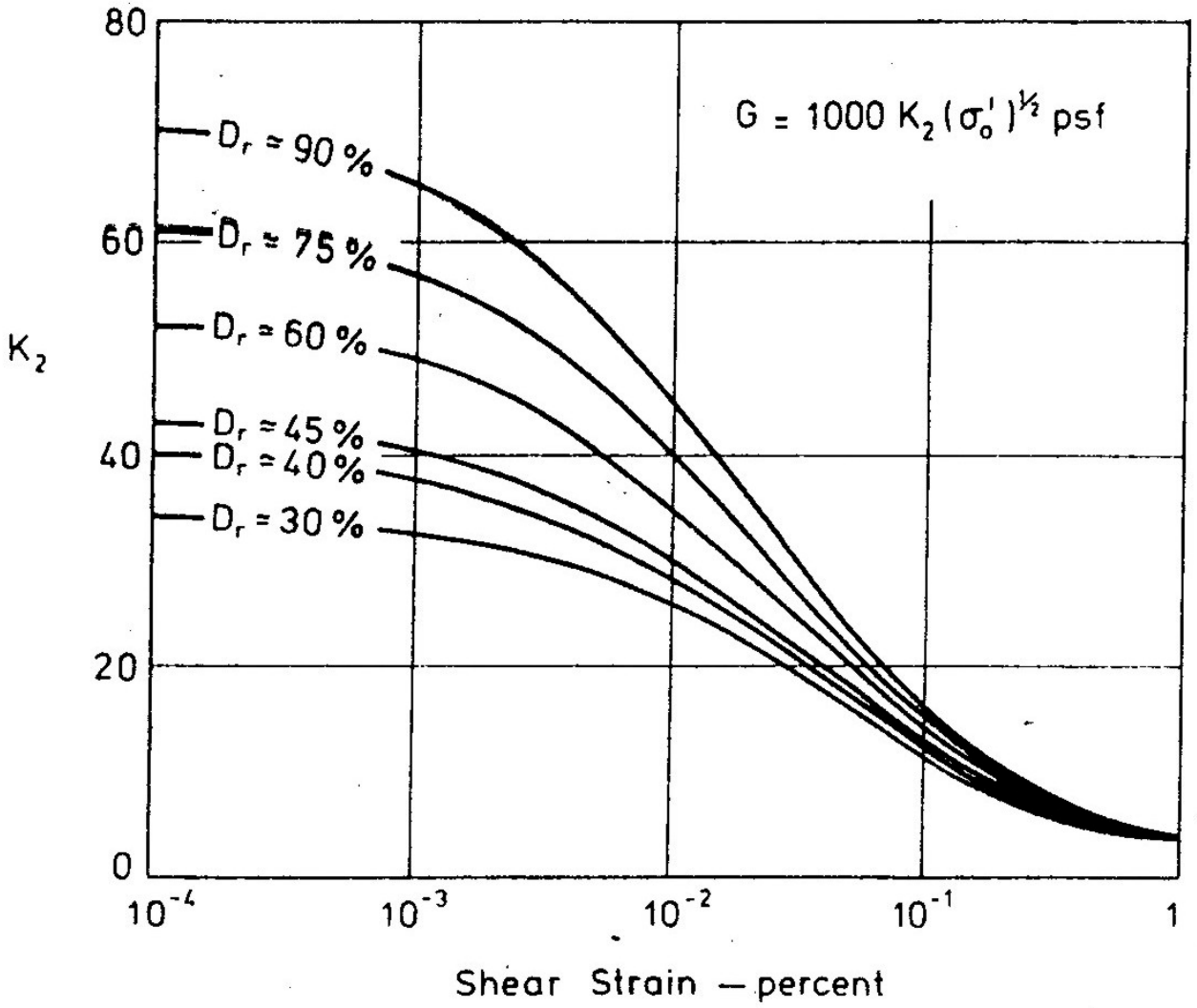

Figure 9.2. Shear moduli of sands at different relative densities (after Seed & Idriss 1970).

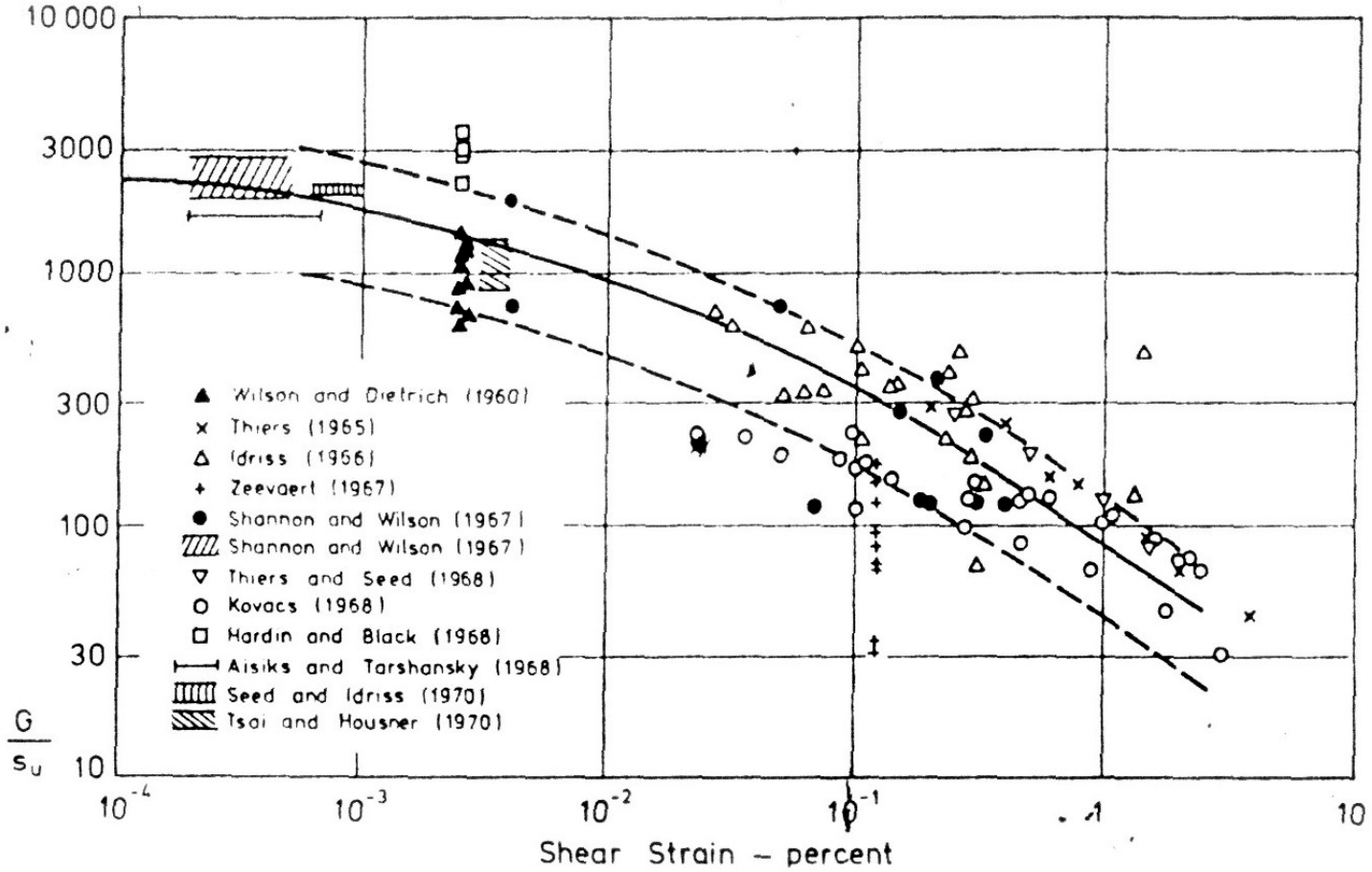

Figure 9.3 In-situ shear moduli for saturated clays (after Seed & Idriss 1970).

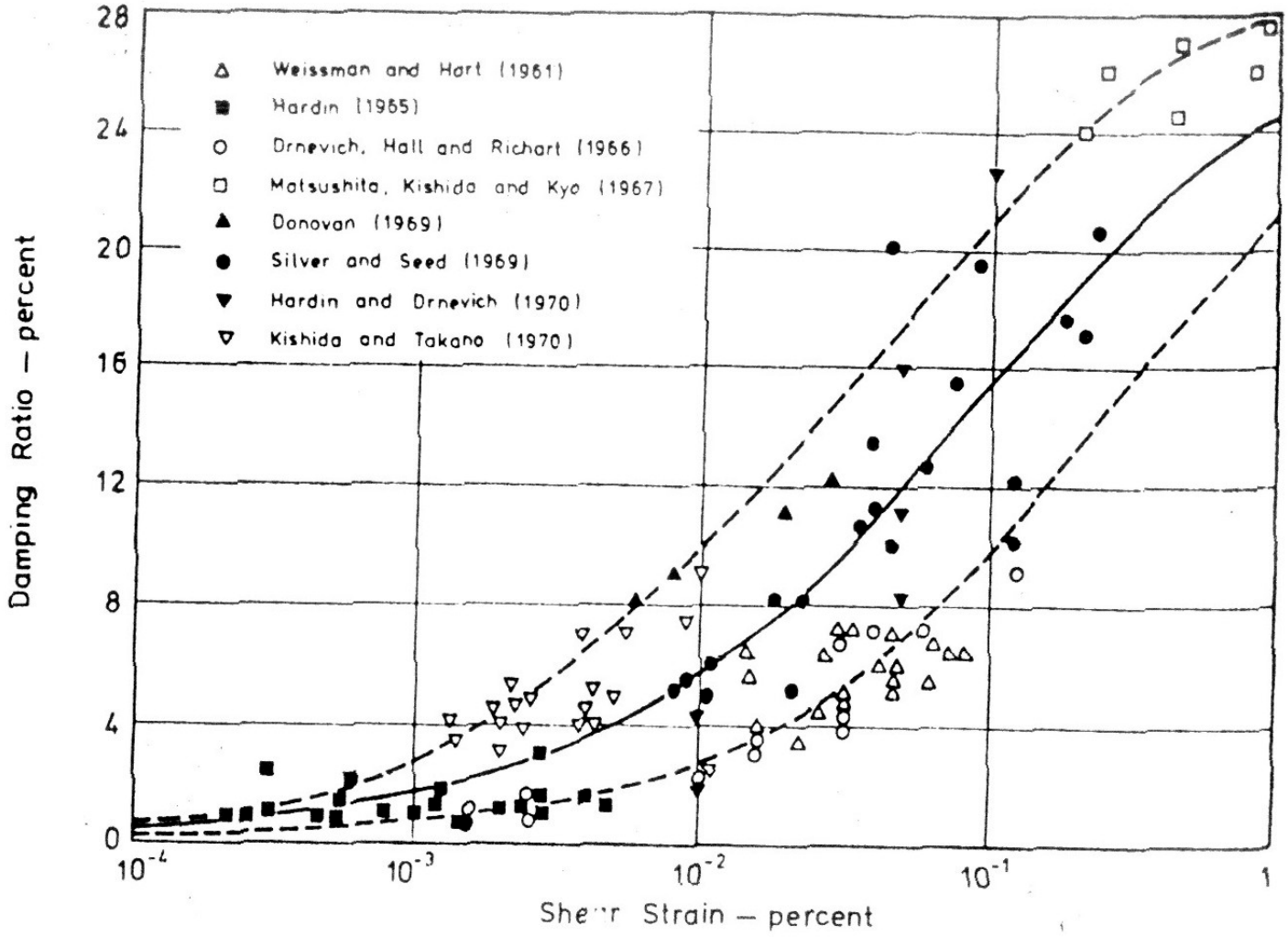

Figure 9.4. Damping ratios for sands (after Seed & Idriss 1970).

Efectos del Confinamiento (1)

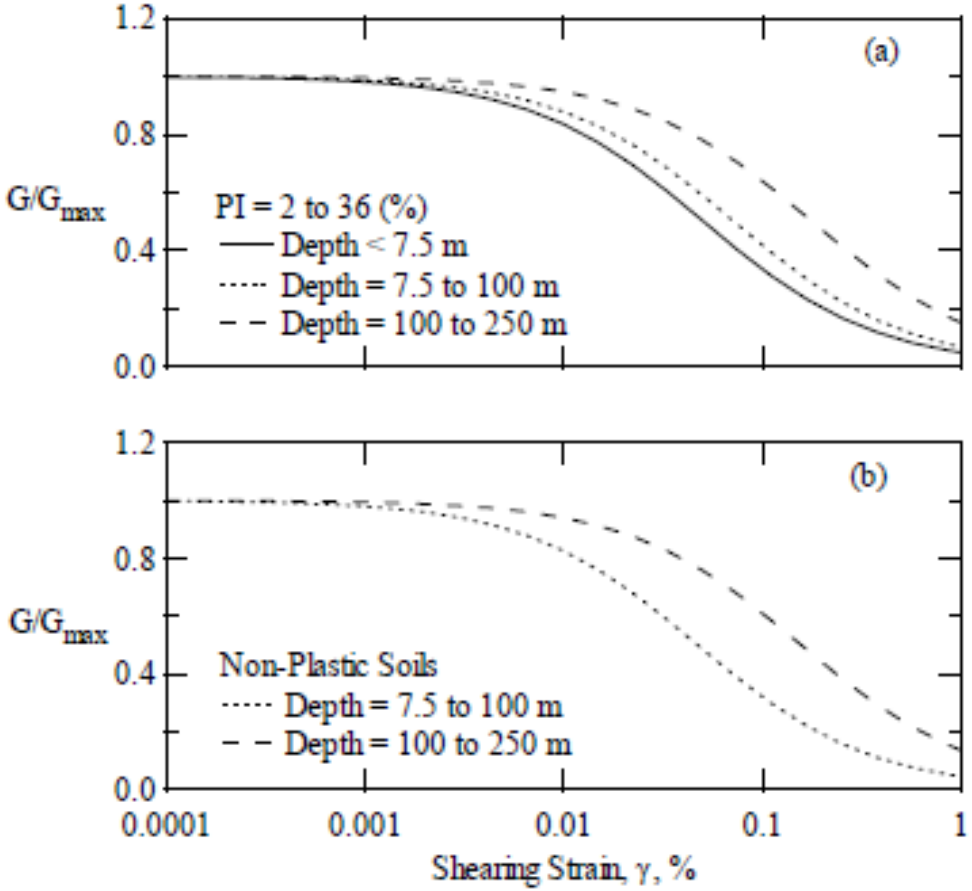

Figure 4.5 The effect of confining pressure on normalized modulus reduction curve (a) for soils with moderate plasticity, and (b) for non-plastic soils evaluated as part of the ROSRINE study (after Stokoe et al., 1999)

(2)

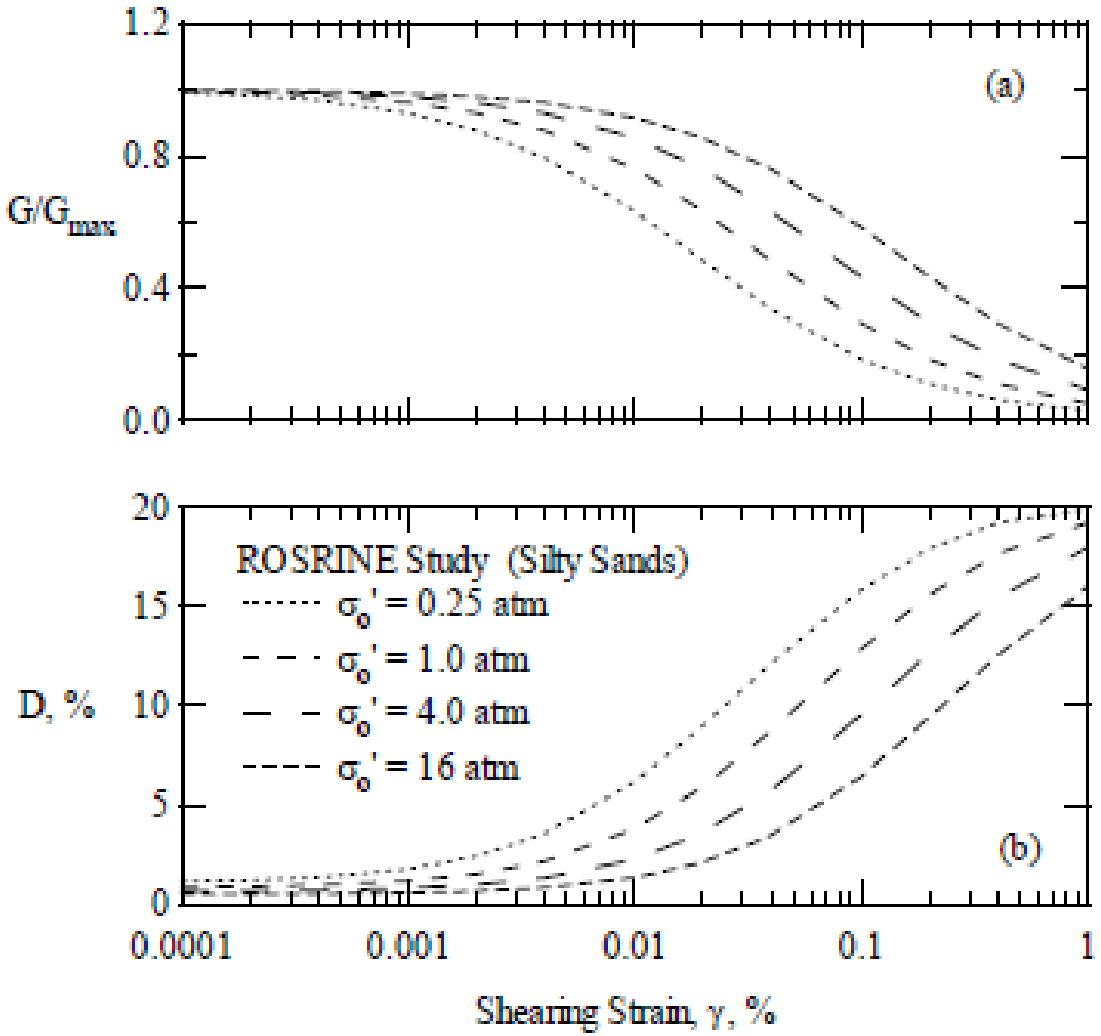

Figure 4.6 The effect of confining pressure on (a) normalized modulus reduction and (b) material damping curves of silty sands evaluated as part of the ROSRINE study (after Darendeli et al., 2001)

Darendeli 2001

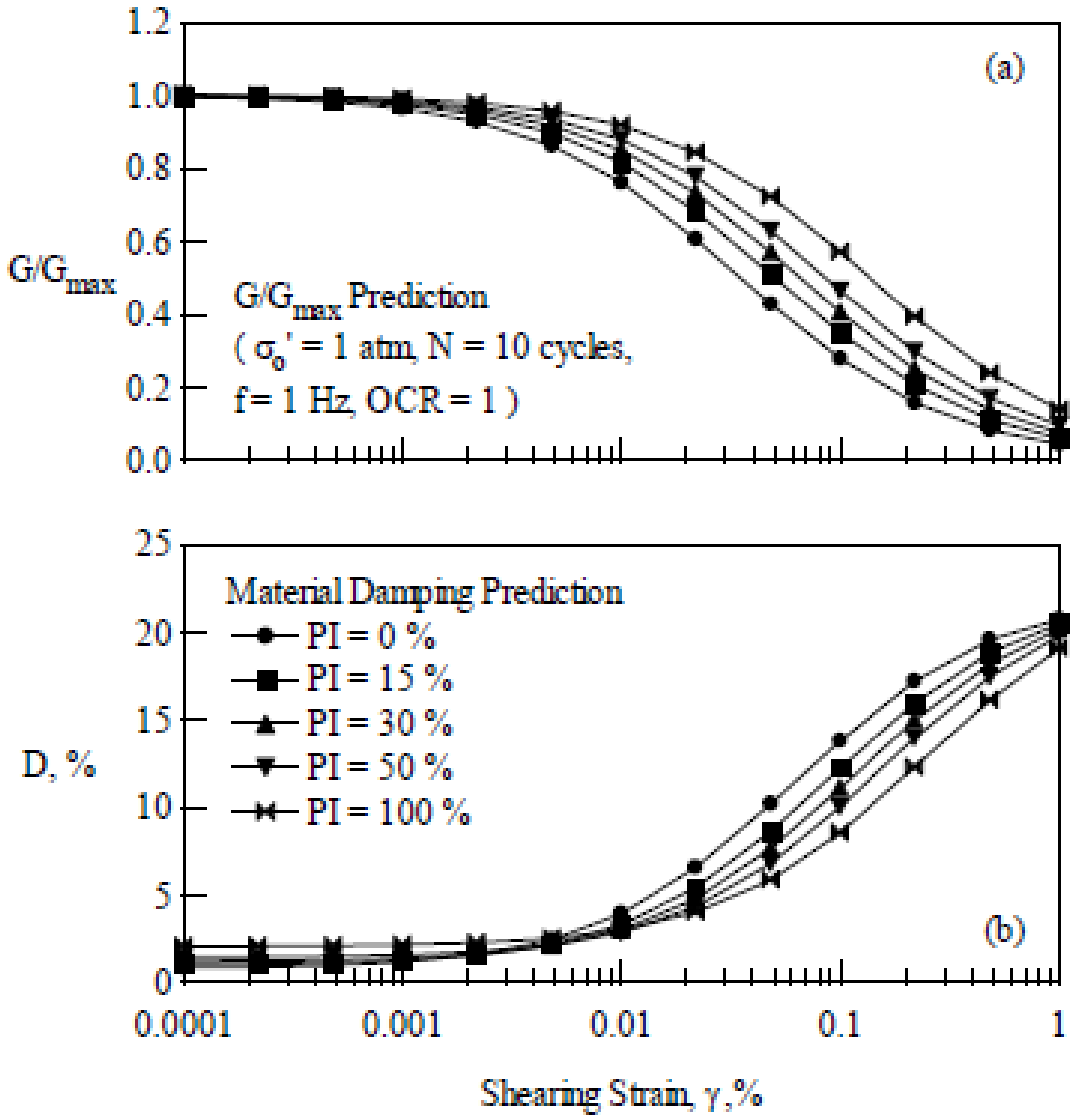

Figure 10.2 Effect of PI on (a) normalized modulus reduction and (b) material damping curves at 1.0 atm confining pressure

Darendeli 2001

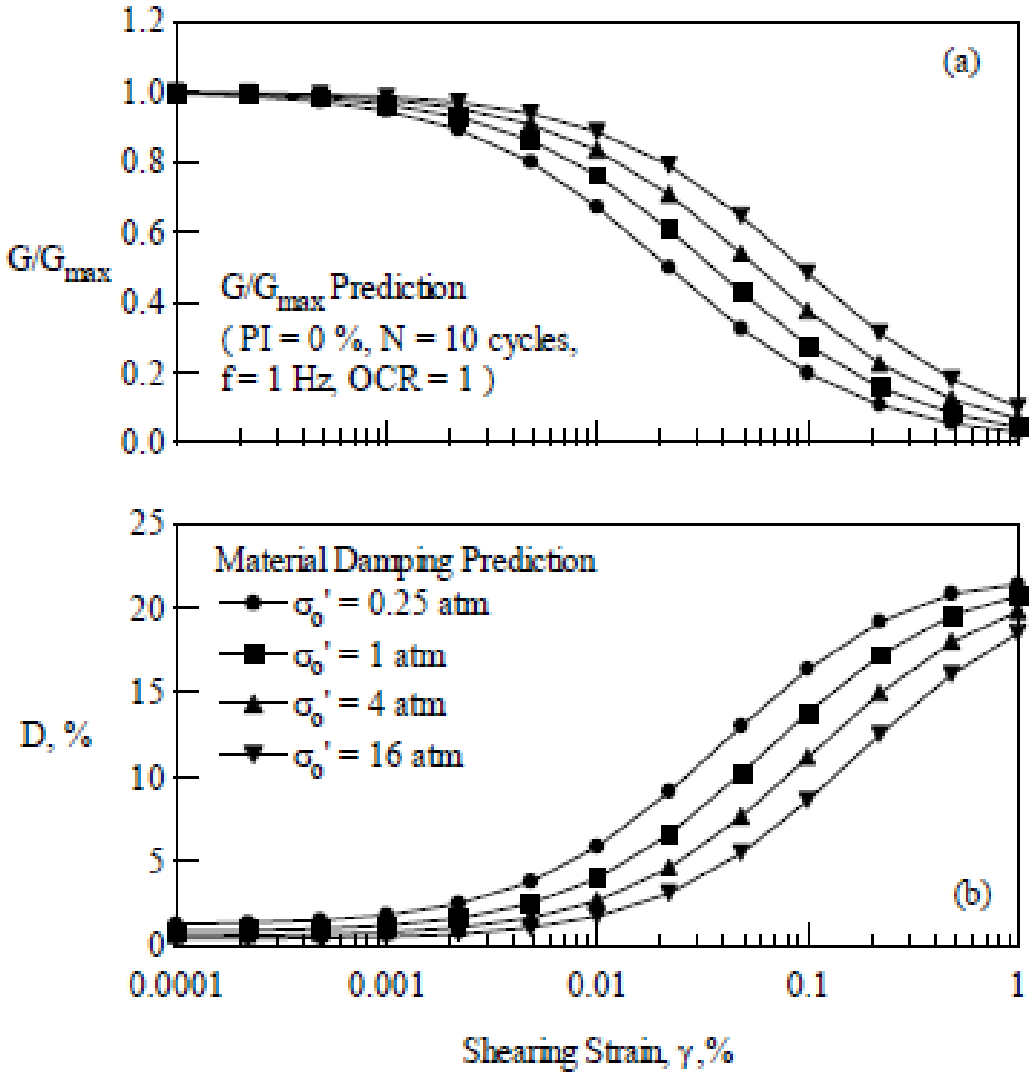

Figure 10.5 Effect of mean effective stress on (a) normalized modulus reduction and (b) material damping curves of a nonplastic soil

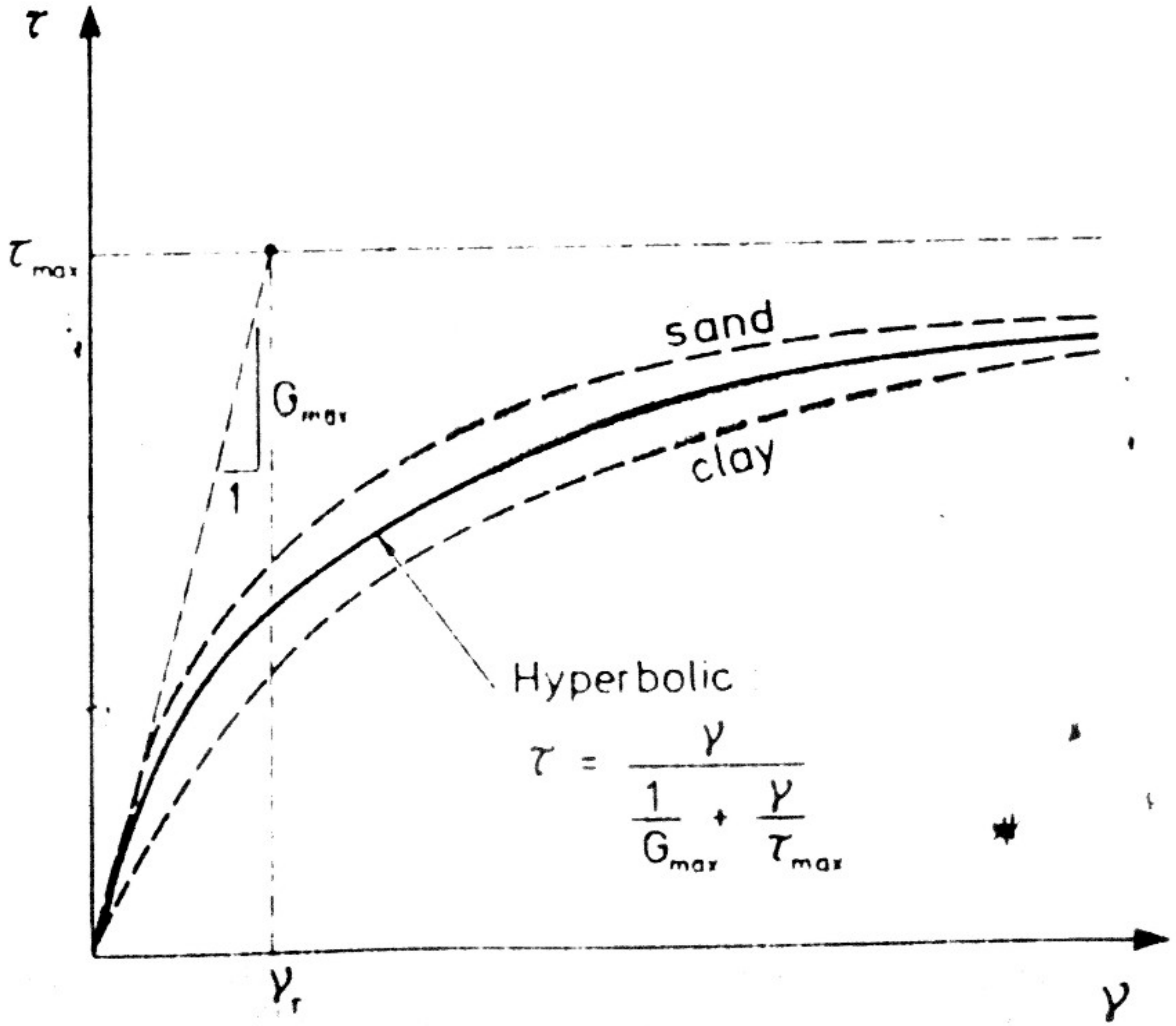

Figure 9.6. Hyperbolic stress–strain relationship (after Hardin & Drnevich 1972b; reprinted by permission of the American Society of Civil Engineers).

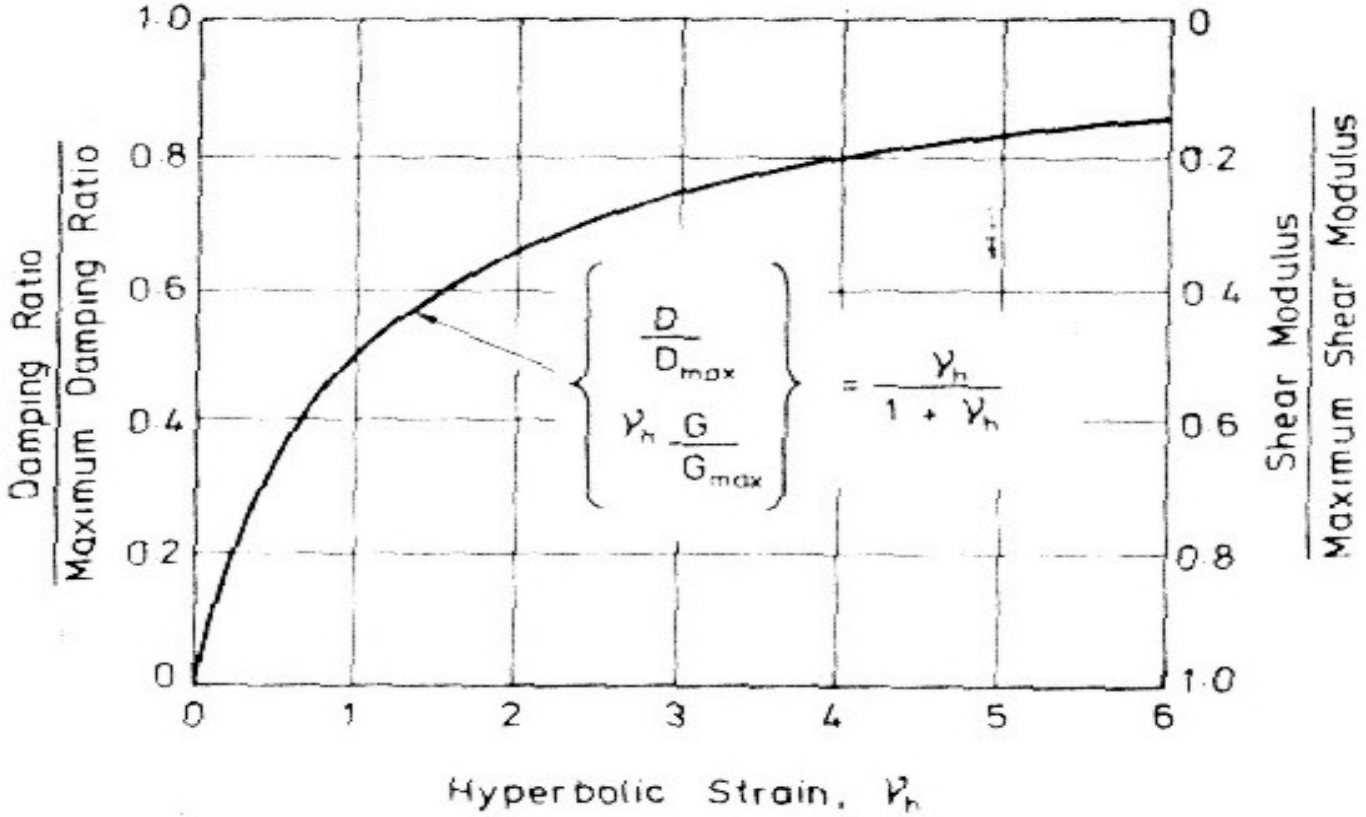

Figure 9.7 Normalized shear moduls and normalized damping ratio versus hyperbolic strain (after Hardin and Drnvech 1972h: reprinted by permision of the American Society of cinvil Engineers)

		a	b	β_{max} (%)
Sable propre sec	Module	-0.5	0.16	
	Amortissement	$0.6\ N^{-1/6} - 1$	$1 - N^{-1/12}$	$33 - 1.5 \log N$
Sable saturé	Module	$-0.2 \log N$	0.16	
	Amortissement	$0.54\ N^{-1/6} - 0.9$	$0.65 - 0.65\ N^{-1/2}$	$20 - 1.5 \log N$
Argile saturée	Module	$1 + 0.25 \log N$	1.3	
	Amortissement	$1 + 0.2\ f^{1/2}$	$0.2\ f\ e^{-\sigma'_m/p_a} + 2.25 \frac{\sigma'_m}{p_a} + 0.3 \log N$	$31 + 1.5\ f^{1/2} - 1.5 \log N - (3 + 0.03\ f) \left[\frac{\sigma'_m}{p_a}\right]^{1/2}$

f = fréquence - Hertz — N = nombre de cycles

σ'_m = contrainte moyenne effective — p_a = pression atmosphérique

Tableau II . Valeurs caractéristiques des paramètres a, b, β_{max}

$$\frac{G}{G_{max}} = \frac{1}{1 + \gamma_h}$$

$$\frac{\beta}{\beta_{max}} = \left[1 - \frac{G}{G_{max}} \right] = \frac{\gamma_h}{1 + \gamma_h}$$

$$\gamma = \frac{\gamma}{\gamma_y} \left[1 + a\ e^{-b\ (\gamma/\gamma_y)} \right]$$

Hardin – Drnevich relationships

Thank you for your attention...